Full-Sky Cosmic-Ray Anisotropy at 10 TeV

Juan Carlos Díaz Vélez

Wisconsin IceCube Particle and Astrophysics Center

The Paris Saclay AstroParticle Symposium 2021

Paris, France

October 19, 2021

Wisconsin IceCube Particle Astrophysics Center

A large-scale ~TeV cosmic ray anisotropy at the level of 10^{-3} has been observed and measured over the last few decades as well as a small-scale structures of angular size from 10° to 30° with an amplitude of 10^{-4}.

North

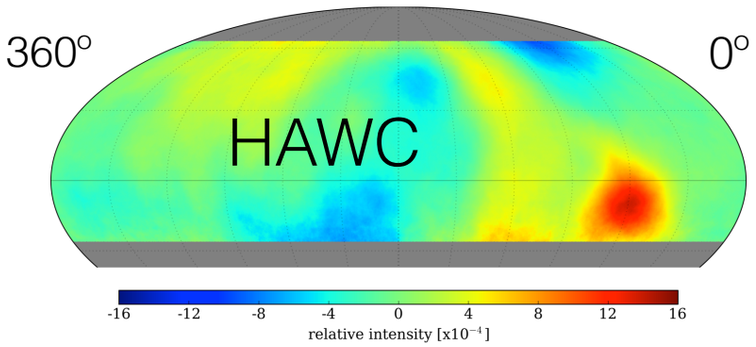

A. U. Abeysekara et al. Astrophys. J. (2014)

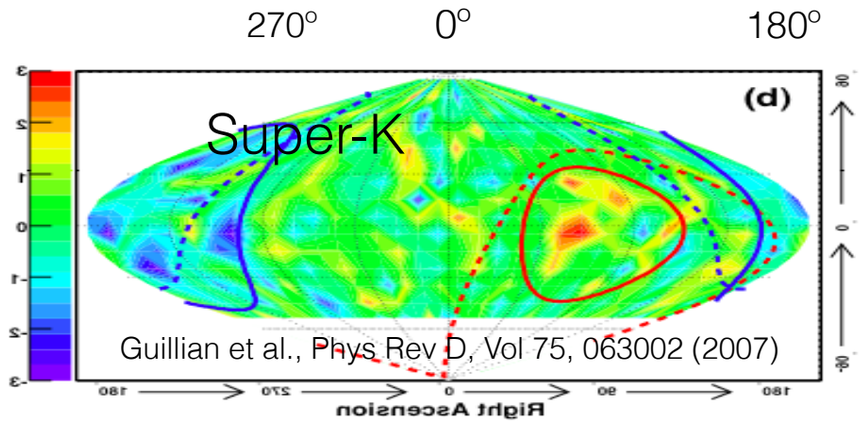

Guillian et al., Phys Rev D, Vol 75, 063002 (2007)

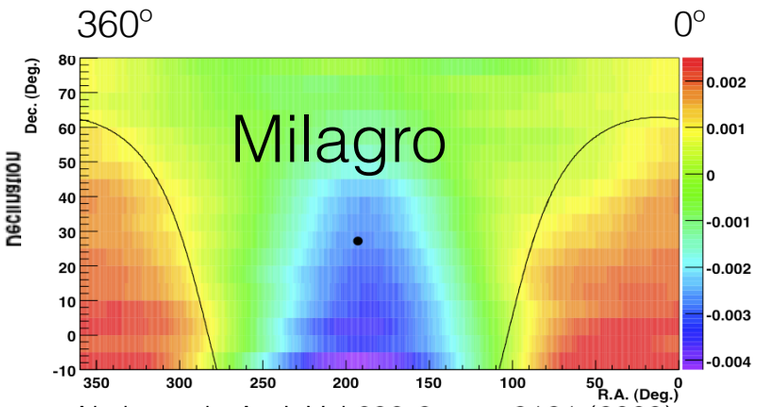

Abdo et al., ApJ, Vol 698-2, pag 2121 (2009)

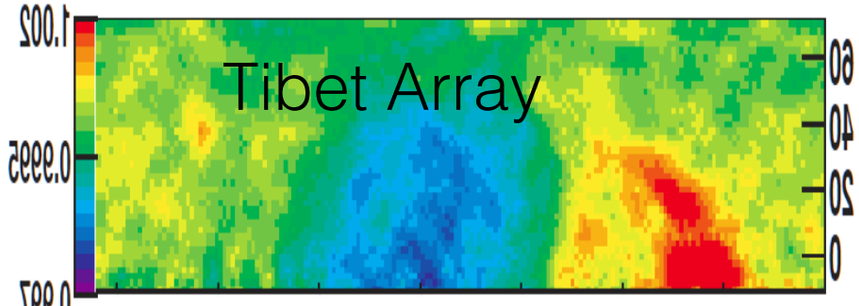

Amenomori et al., Science Vol. 314, pp. 439 (2006)

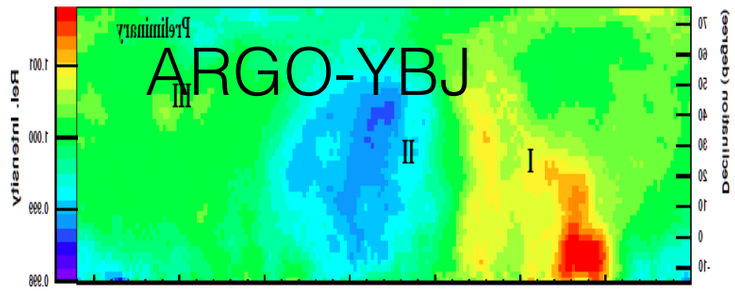

Zhang et al. Proc. 32nd ICRC (2009)

360° 0°

South

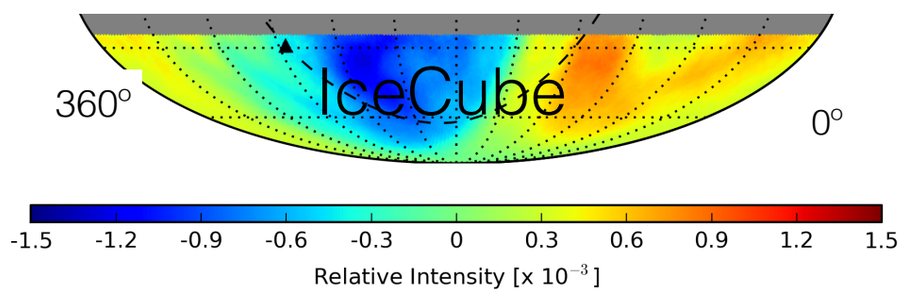

M. G. Aartsen et al. Astrophys.J. 826 (2016)

A number of observatories in the North and only IceCube in the southern hemisphere.

Ground Observation Biases

- Limited FoV in time-integrated methods can attenuate large-scale (dipole, quadrupole) features.
- Partial sky coverage leads to correlations across multiple components in spherical harmonic decomposition.
- Ground-based observatories have poor energy and mass resolution.
- Blindness to vertical dipole component δ_N from time integration.
- Reconstruction biases can also limit our ability to correctly reconstruct the pitch angle distribution of cosmic rays in the interstellar medium.
- Interference across reference frames can result in biases on the measurement of dipole component.
- These biases can limit our ability to interpret results.

Method for measuring CR anisotropy

1 Build a binned data map using the equatorial coordinates of the events

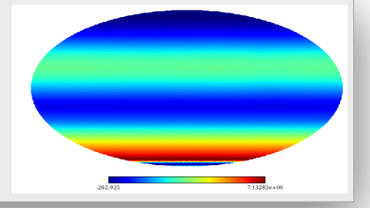

2 Construct a “reference” map by integrating acceptance over 24 hours.

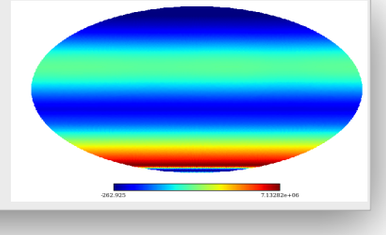

Time-scrambling:

$$(\theta, \phi, t) \rightarrow (\alpha, \delta)$$
$$(\theta, \phi, t') \rightarrow (\alpha', \delta')$$

Direct integration:

$$\langle N(\alpha, \delta) \rangle = \int dt \int d\Omega A(ha, \delta) \cdot R(t) \cdot \epsilon(ha, \alpha, t)$$

3 Correlate pixels to increase sensitivity to different angular scales

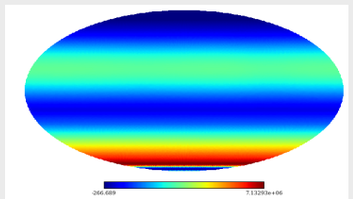

Relative Intensity

$$\delta I(\alpha, \delta)_i = \frac{N(\alpha, \delta)_i - \langle N \rangle(\alpha, \delta)_i}{\langle N \rangle(\alpha, \delta)_i}$$

4 Calculate relative differences between data and reference with significance.

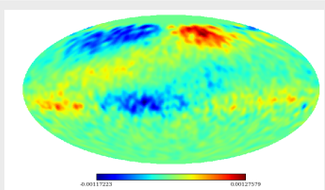

$$s_i = \sqrt{2} \left\{ N_i \log \left[\frac{1+\alpha}{\alpha} \left(\frac{N_i}{N_i + N_o} \right) \right] + N_o \log \left[(1+\alpha) \left(\frac{N_o}{N_i + N_o} \right) \right] \right\}^{1/2}$$

5 Calculate statistical significance for each pixel

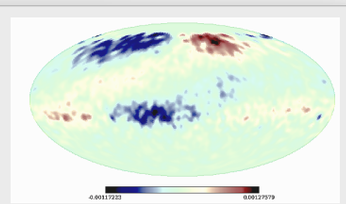

Relative Intensity

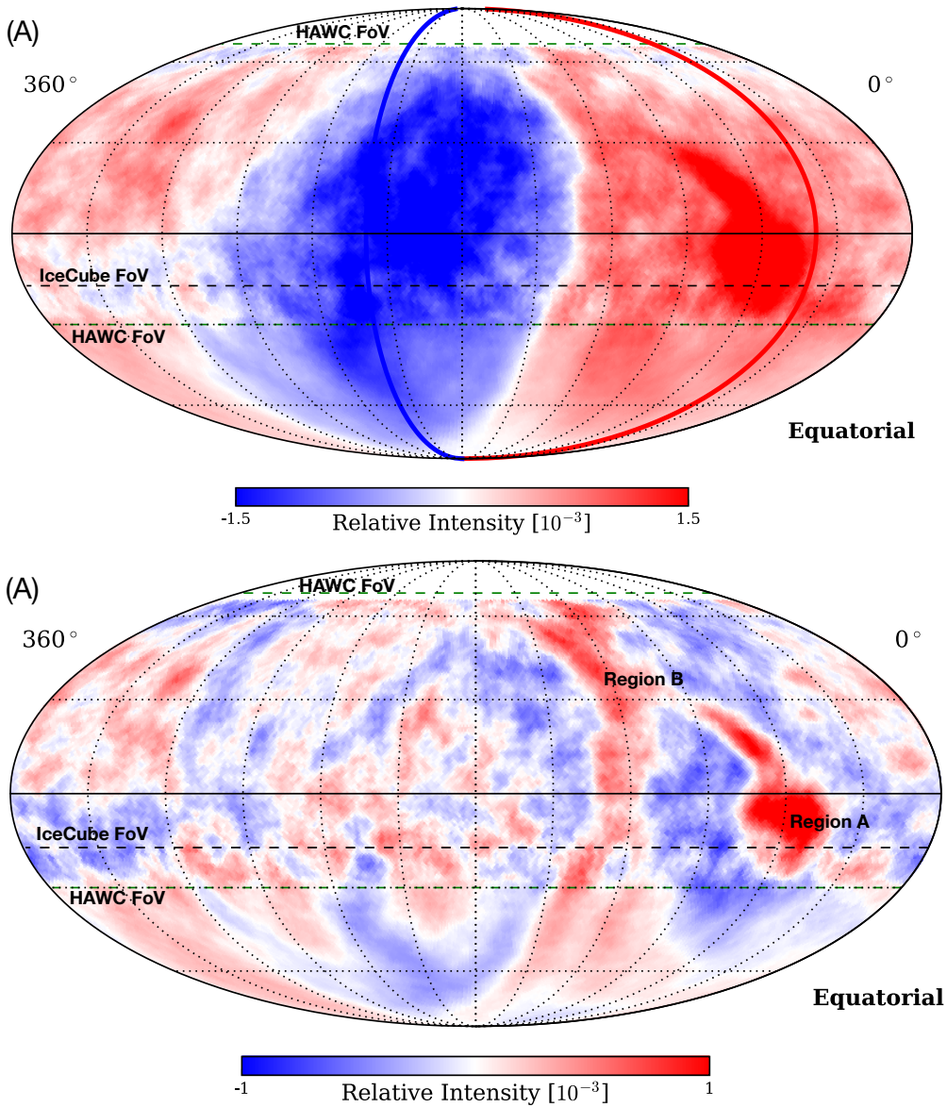

Li-Ma Statistical Significance

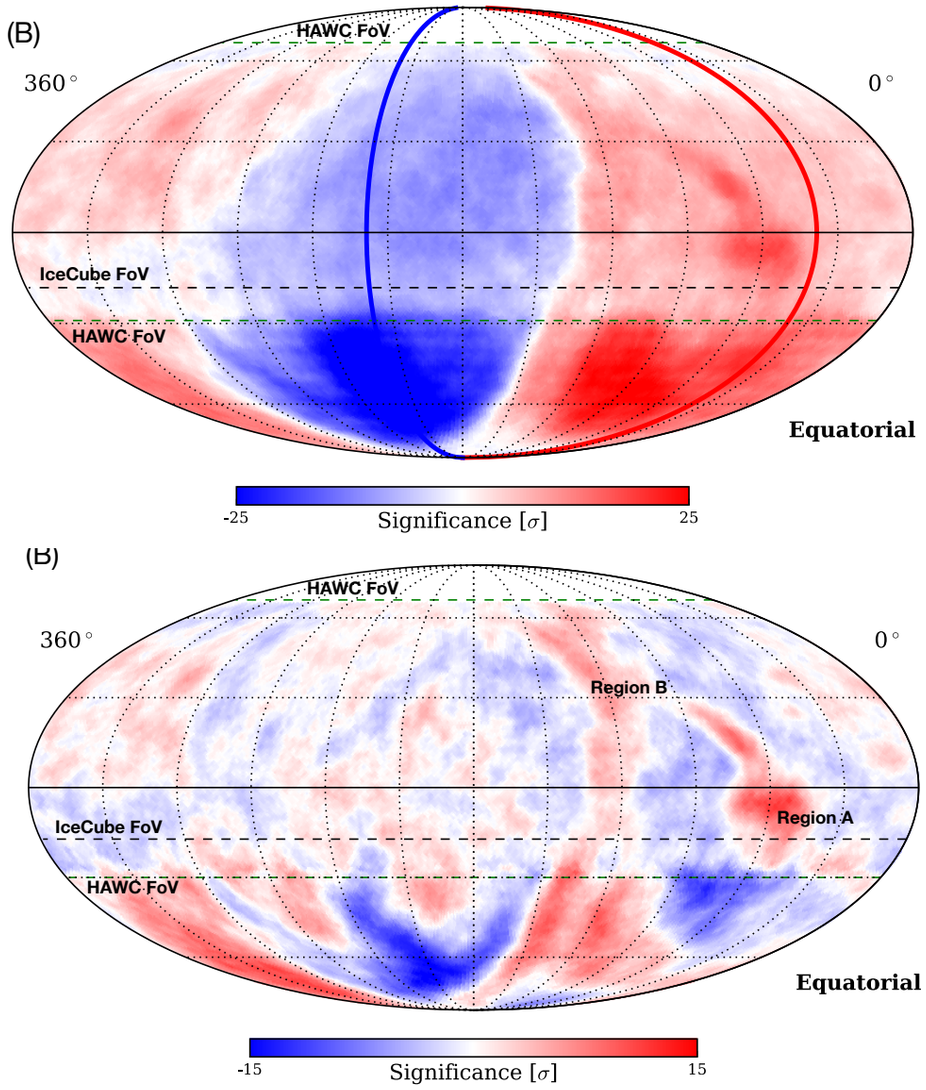

A. U. Abeysekara *et al* 2019 *ApJ* **871** 96

Combined measurement of Cosmic-Ray Anisotropy by IceCube and HAWC at 10 TeV.

The higher significance of structures in the southern hemisphere reflects the higher larger statistics of the IceCube dataset.

Limited FoV in Time-Integrated Methods

- Traditional time-integration methods can strongly attenuate large-scale structures exceeding the size of the instantaneous field of view for detectors located at mid latitudes.
- A fixed position on the celestial sphere is only observable over a limited period every day. The total number of cosmic ray events from a fixed position can only be compared against reference data observed during the same period that can lead to an under- or overestimation of the isotropic reference level.

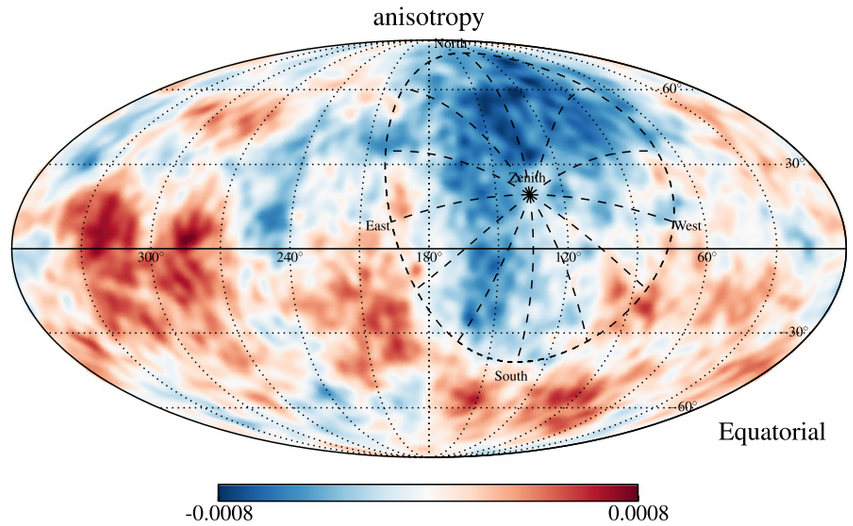

M. Ahlers et al (arXiv:1601.07877)

Iterative maximum likelihood method

Ahlers, BenZvi, Desiati, Díaz-Vélez, Fiorino & Westerhoff 2016 *ApJ* **823** 10

The likelihood of observing n cosmic rays is given by the product of Poisson probabilities

$$\mathcal{L}(n|I,\mathcal{N},\mathcal{A}) = \prod_{\tau i} \frac{(\mu_{\tau i})^{n_{\tau i}} e^{-\mu_{\tau i}}}{n_{\tau i}!}$$

relative intensity

relative acceptance

$$\mu_{\tau i} \simeq I_{\tau i} \mathcal{N}_{\tau} \mathcal{A}_i$$

expected number of events from isotropic background

Angular Power Spectrum

IceCube (6-years)

Angular power spectra for the relative intensity map for six years of IceCube data; before and after the subtraction of the best-fit dipole and quadrupole terms.

This measurement would suggest that the quadrupole component is stronger than the dipole component.

M. G. Aartsen *et al* 2016 *ApJ* **826** 220

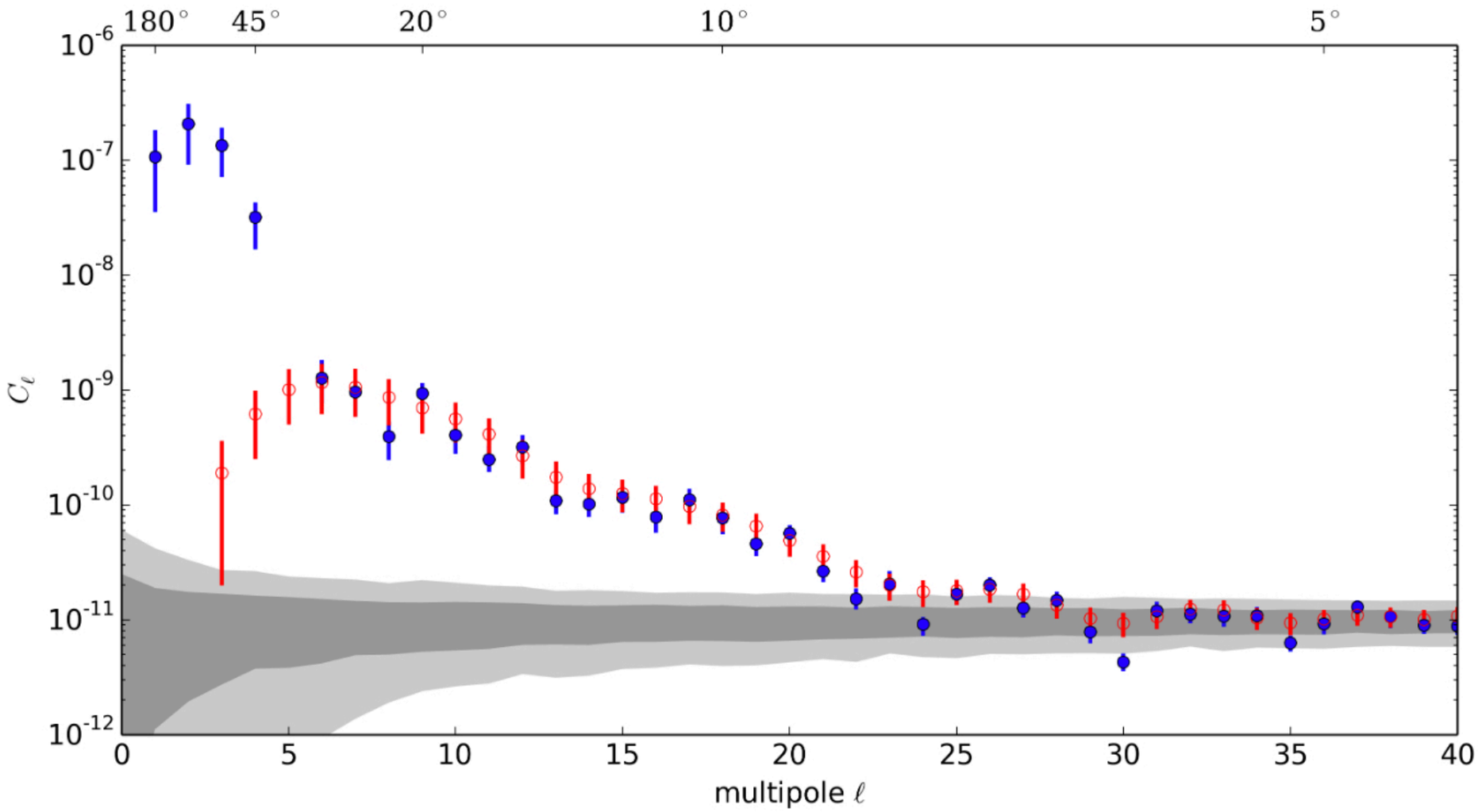

Angular Power Spectrum

HAWC (2-years)

Angular power spectra for the relative intensity map for two years of HAWC data.

Here we see a much larger dipole component compared to the quadrupole, and compared to the IceCube measurement.

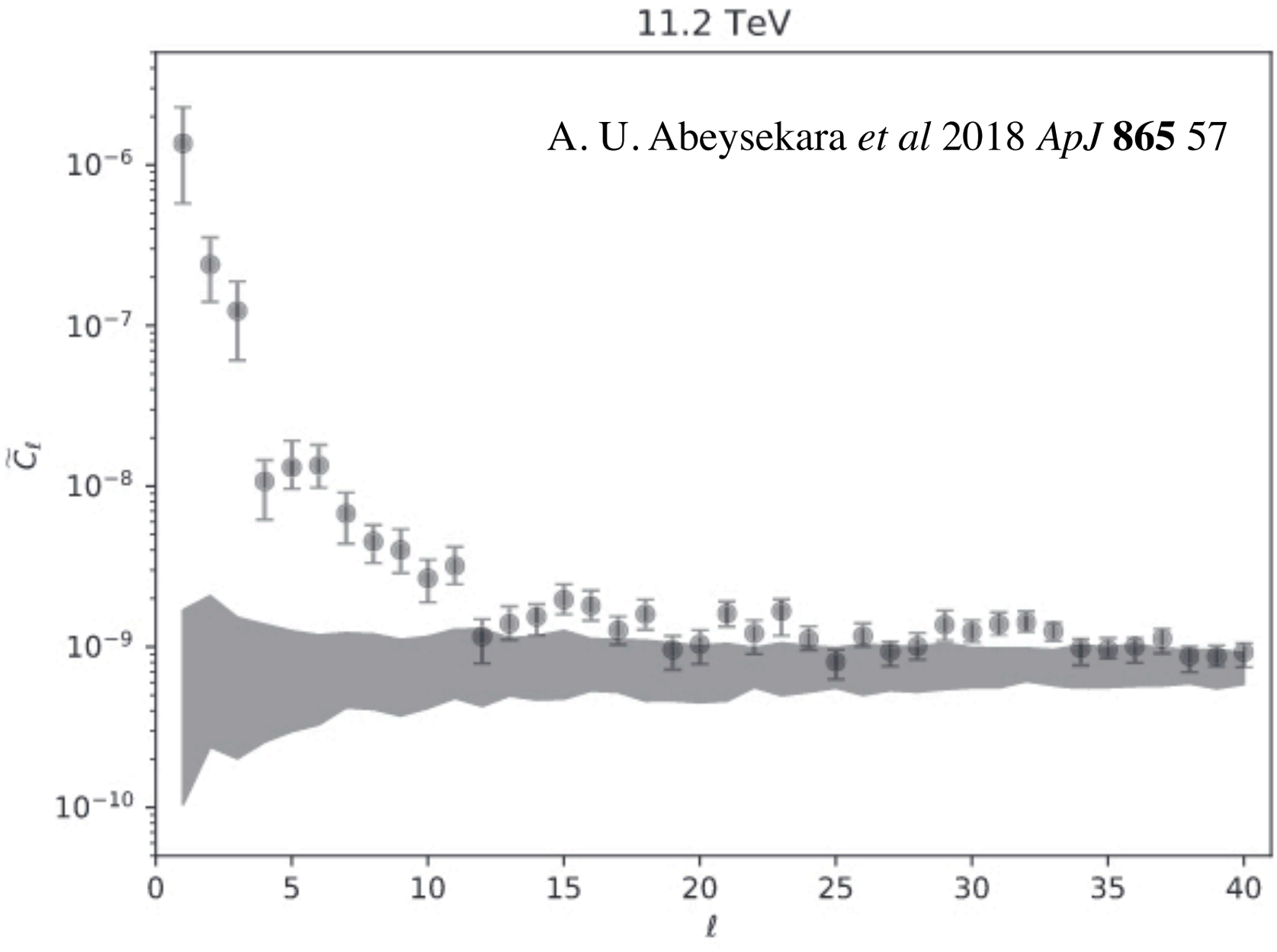

Full-Sky Angular Power Spectrum

A. U. Abeysekara *et al* 2019 *ApJ* **871** 96

- Iterative method recovers most of the power of large scale structure in mid-latitude observatories like HAWC.
- The highest angular power for $\ell = 1$ is obtained with the greater sky coverage from combining data from both observatories and reconstruction with the iterative method.
- The larger sky-coverage in the HAWC-IceCube measurement disambiguates power between ℓ -modes

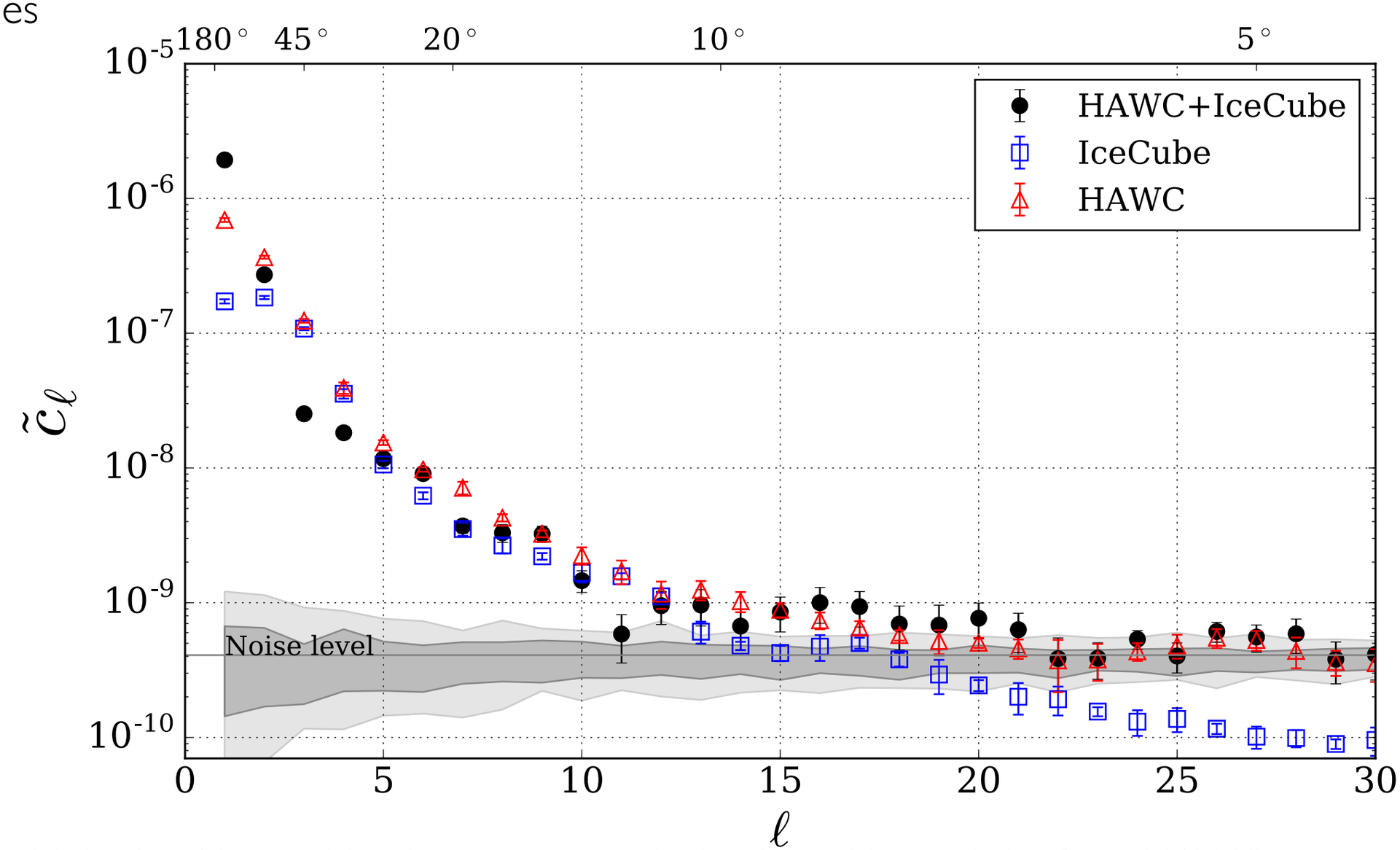

*Noise level in combined measurement is dominated by statistics from HAWC

Partial sky-coverage

Pure dipole (3d sensitivity)

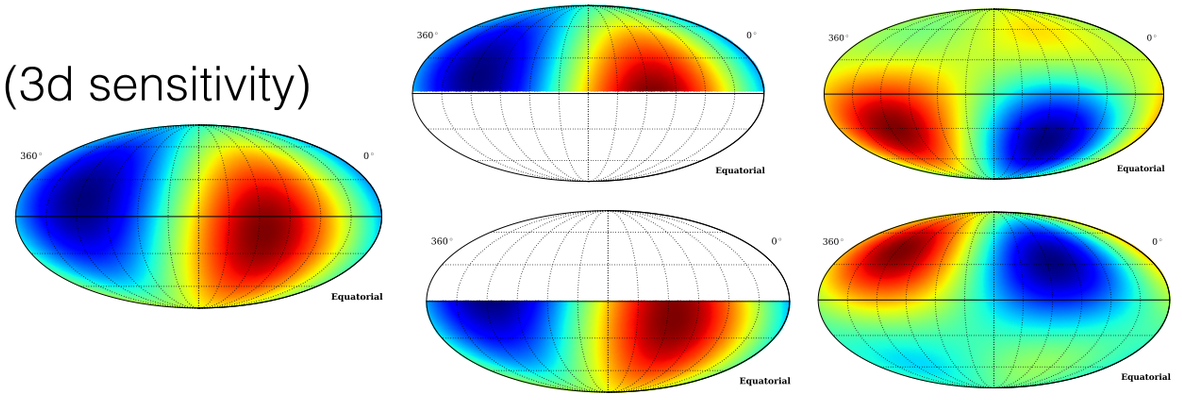

Multipole components are subject to crosstalk caused by partial sky coverage since there is a degeneracy between different ℓ-modes.
A purely dipole can result in an artificial quadrupole due to partial sky coverage.

A. U. Abeysekara *et al* 2019 *ApJ* **871** 96

δ_{6h}=0.0015, δ_{0h}=0, δ_N=0

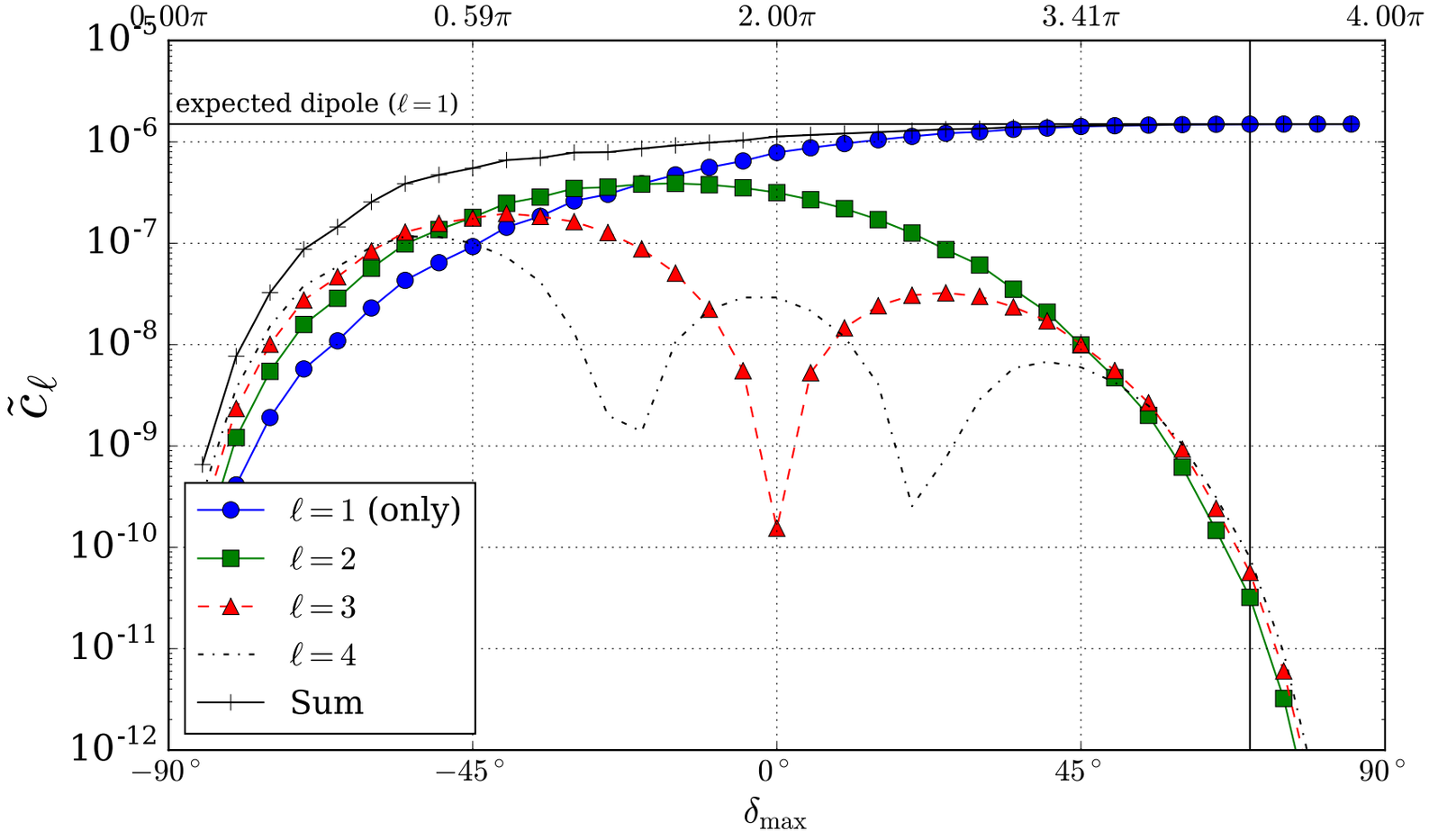

Partial sky-coverage

A. U. Abeysekara *et al* 2019 *ApJ* **871** 96

Multipole components are subject to crosstalk caused by partial sky coverage since there is a degeneracy between different ℓ-modes.

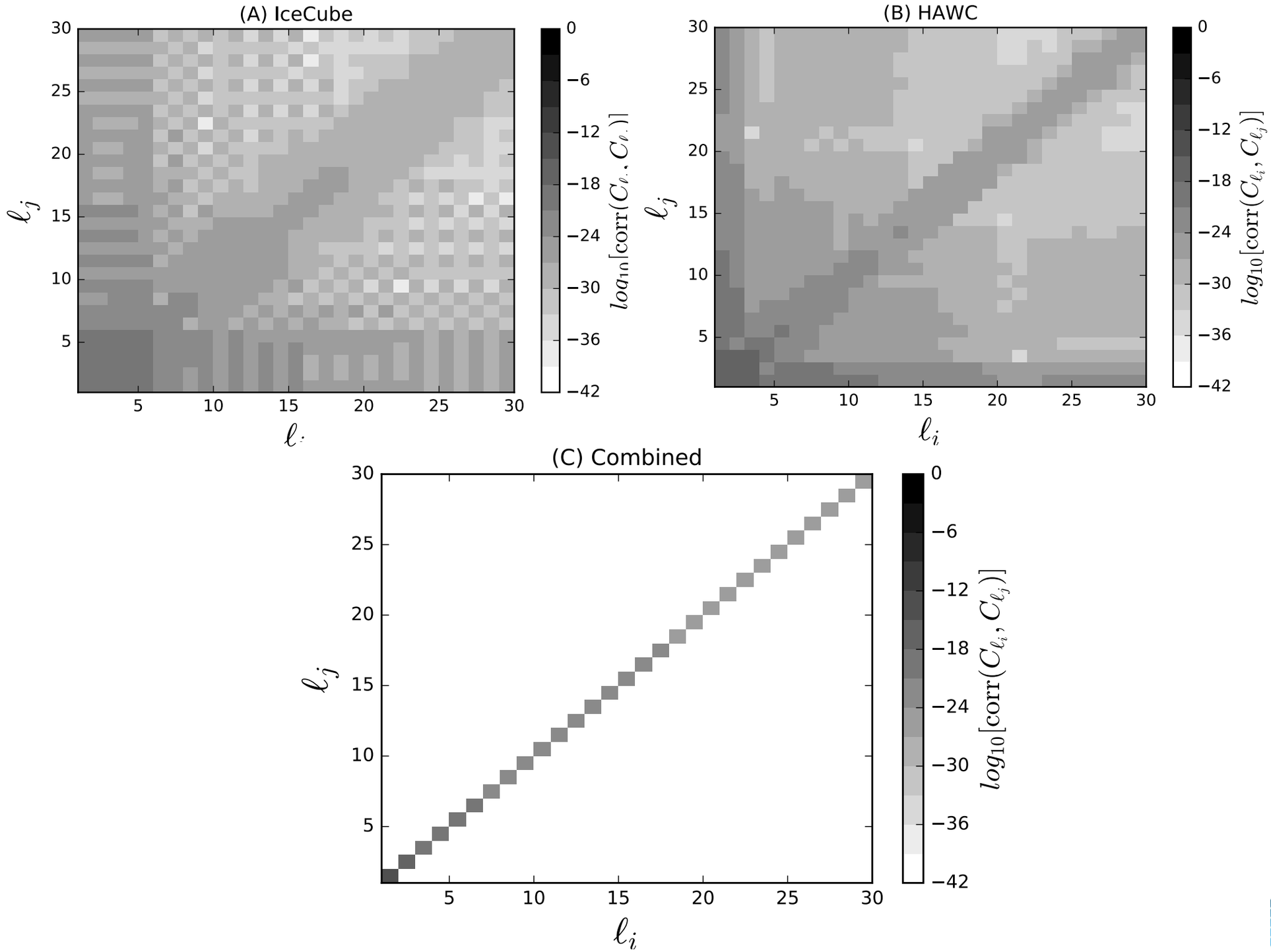

Horizontal projection

A. U. Abeysekara *et al* 2018 *ApJ* **865** 57

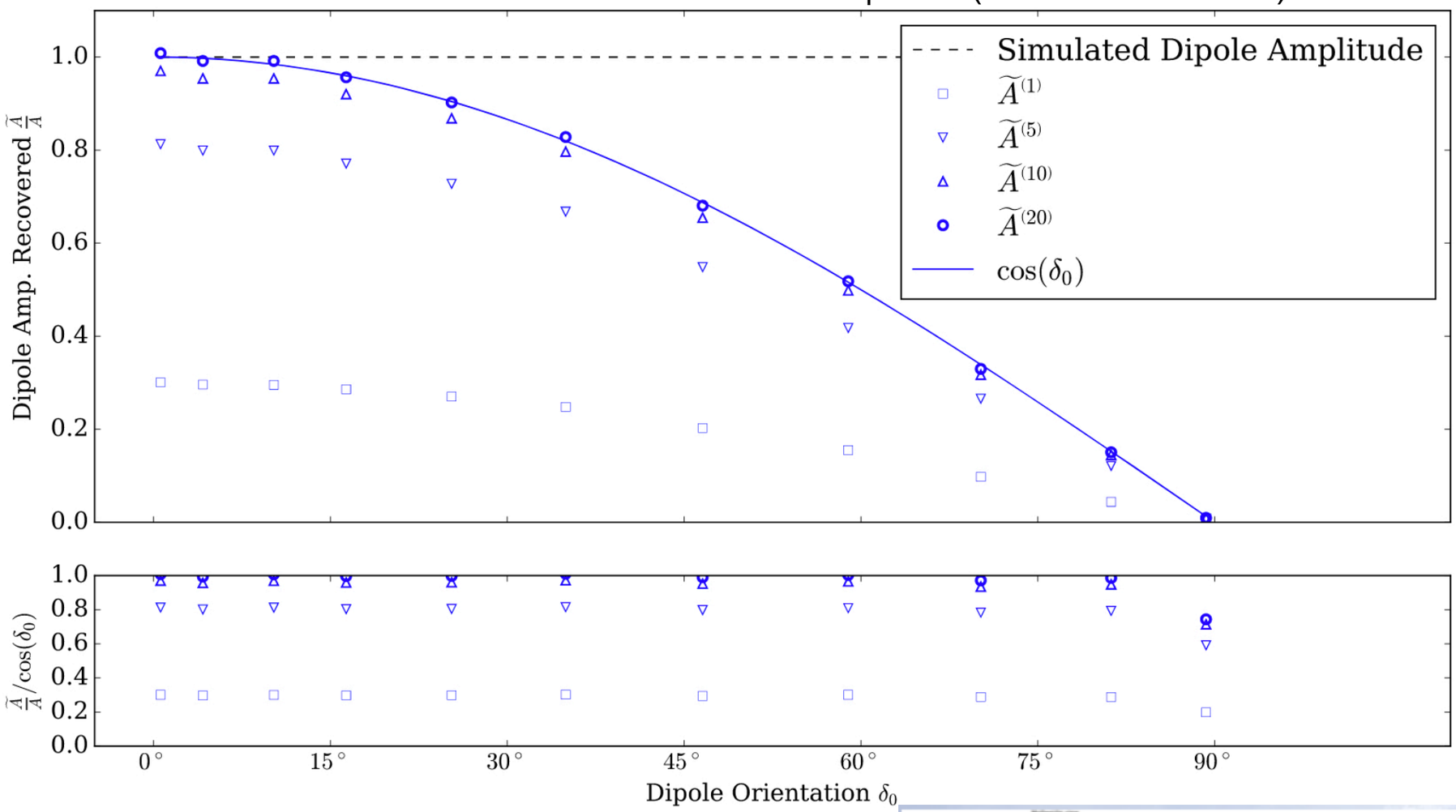

- Simulated dipole reconstructed with LLH method.
- Solid line is best possible with ground-based observations.
- Method improves with iteration (light to dark red).
- Geometric correction needed due to limited sky coverage.

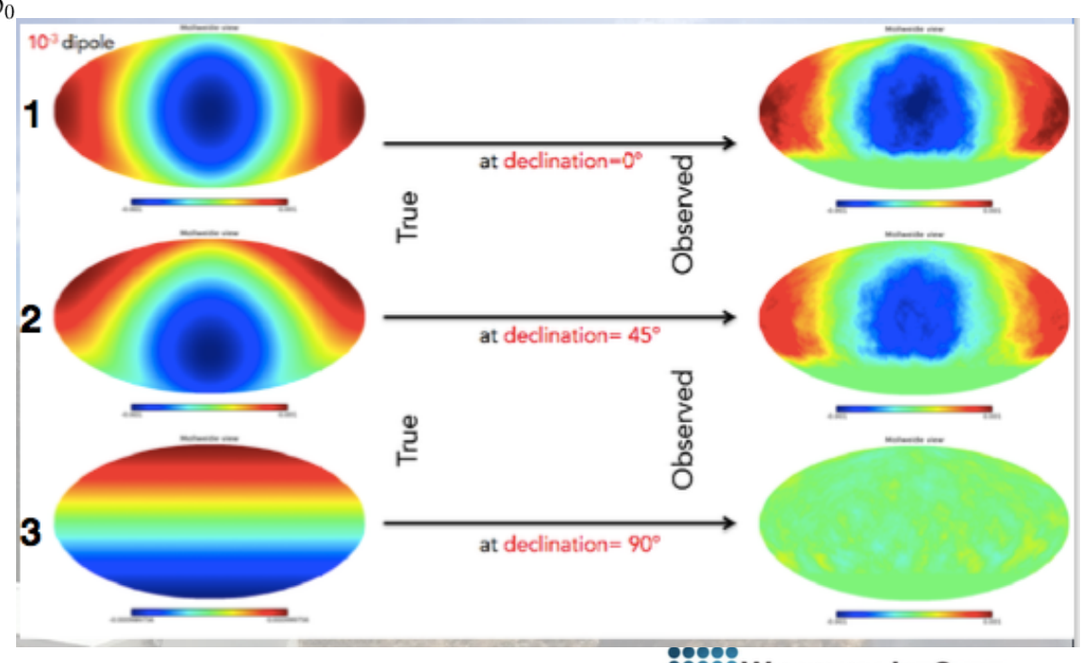

Dipole Component

A. U. Abeysekara *et al* 2019 *ApJ* **871** 96

δ_{0h} and δ_{6h} are the dipole components parallel to the equatorial plane and pointing to the direction of the local hour angle 0h ($\alpha = 0°$) and 6h ($\alpha = 90°$) of the vernal equinox, respectively. Ground-based observatories are not sensitive the dipole component pointing north δ_N.

A_1 = 1.17e-3 ± 5.8e-6

$\boldsymbol{\alpha}_1$ = 38.4° ± 0.3°

$\boldsymbol{\delta}_{0h}$ = 9.16e-4 ± 0.04e-4

$\boldsymbol{\delta}_{6h}$ = 7.25e-4 ± 0.04e-4

$\boldsymbol{\delta}_N$ = ?

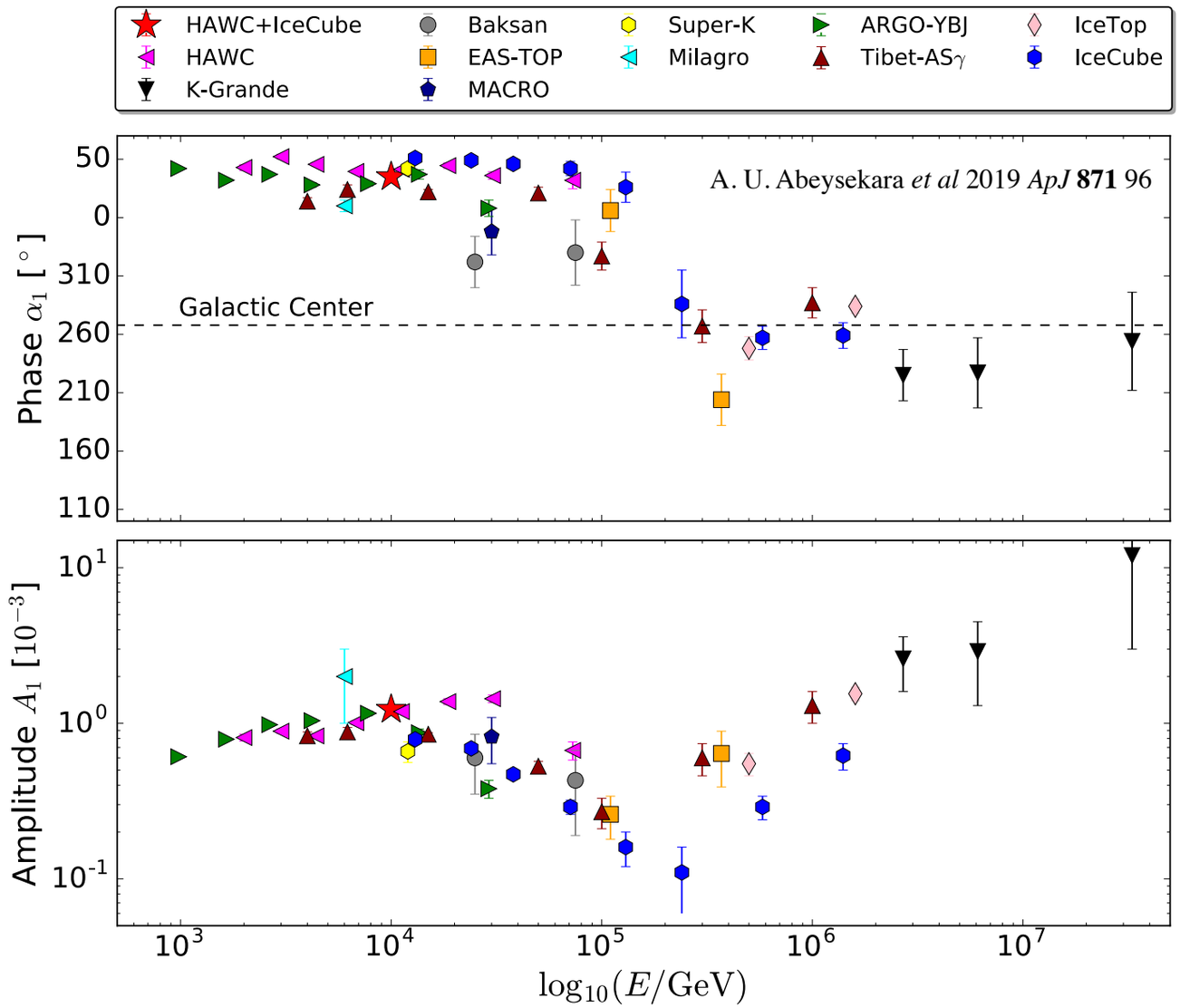

Estimation of the Local Interstellar Magnetic Field

A. U. Abeysekara *et al* 2019 *ApJ* **871** 96

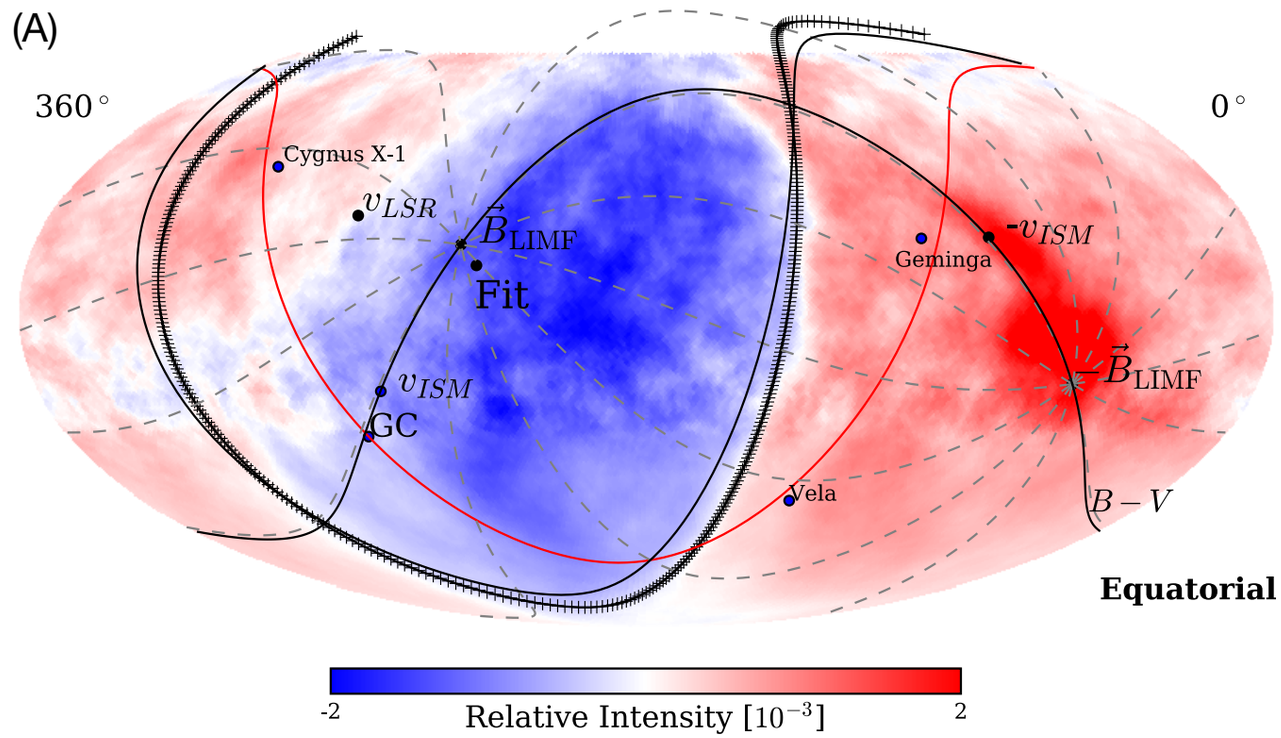

χ^2 distribution map for circular fit to boundary between large-scale excess and deficit regions. The black point corresponds to the minimum χ^2 for the center of the circle and the black curve is the fitted circle. The gray points are the selected pixels for the fit. The best fit has a value of χ^2/ndof = 585/579.

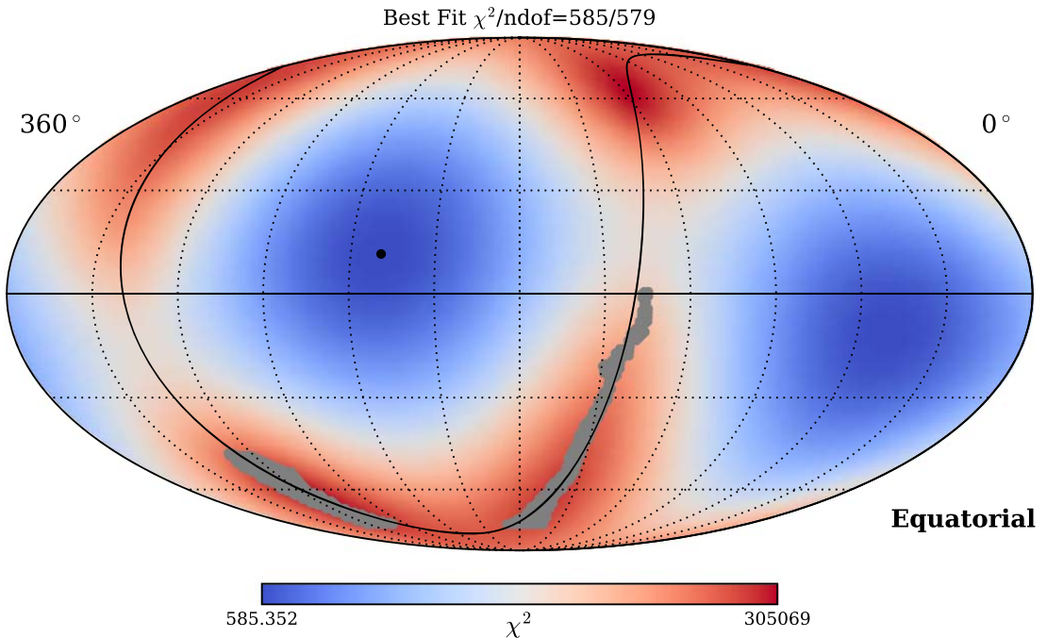

Estimation of the Local Interstellar Magnetic Field

A. U. Abeysekara *et al* 2019 *ApJ* **871** 96

Inferred direction obtained for the local interstellar magnetic field $\mathbf{B}_{\mathrm{LIMF}}$:

229°.2 ± 3°.5 R.A.
11°.4 ± 3°.0 decl.

From which a value for the vertical dipole vector component is obtained assuming the dipole points in the direction of $\mathbf{B}_{\mathrm{LIMF}}$

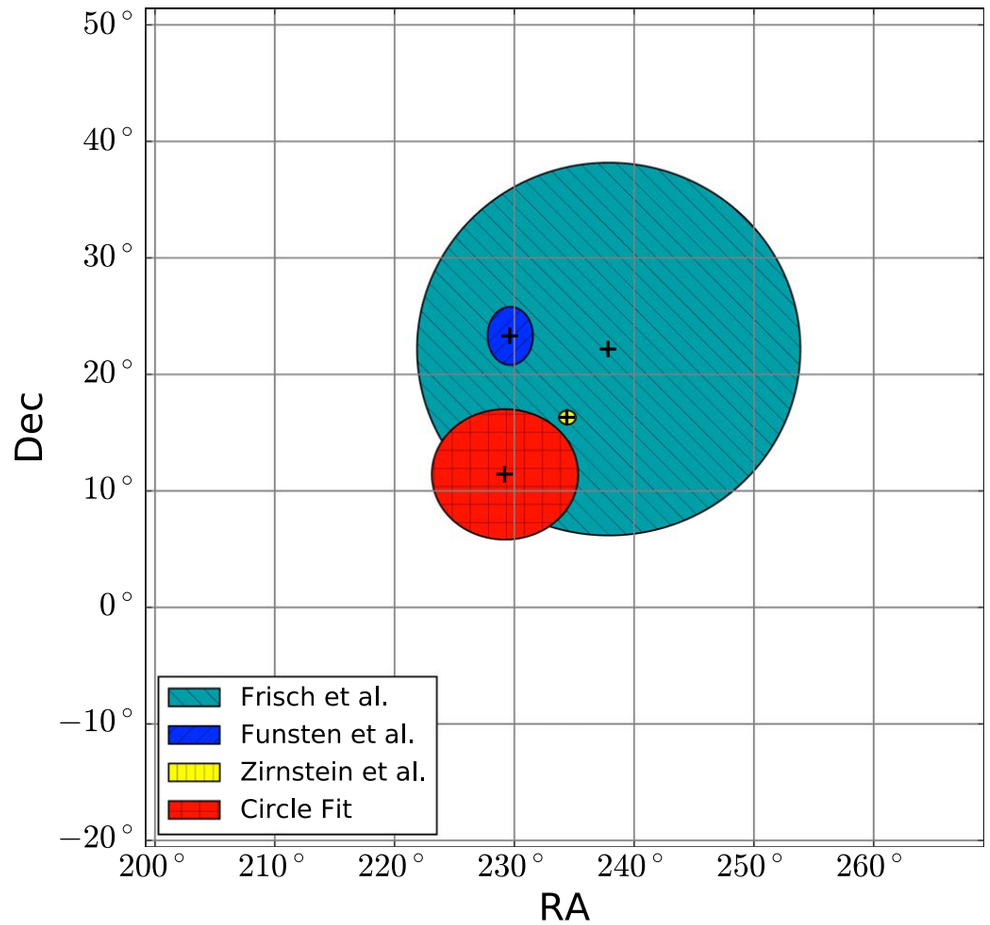

$\delta_N \sim -3.97\ ^{+1.0}_{-2.0} \times 10^{-4}$

Circular fit to boundary between large-scale excess and deficit regions in J2000 equatorial coordinates, along with magnetic field measurements done through different methods.

Lensing effect from the Heliosphere

Díaz-Vélez & Desiati, PoS(ICRC2019)1076

The Larmor radius of a particle with energy E and charge z in a magnetic field of magnitude B is given by

$$R_L \simeq \frac{220}{z}\left(\frac{E}{1\mathrm{TeV}}\right)\left(\frac{1\mu\mathrm{G}}{B}\right)[\mathrm{AU}]$$

For particles with rigidity of 1 TV in with B ~ 3 μG, the gyroradius, R_L ~ 73 AU. For 10 TV particles, R_L ~ 730 AU is the same order of magnitude of the transverse size of the heliosphere.

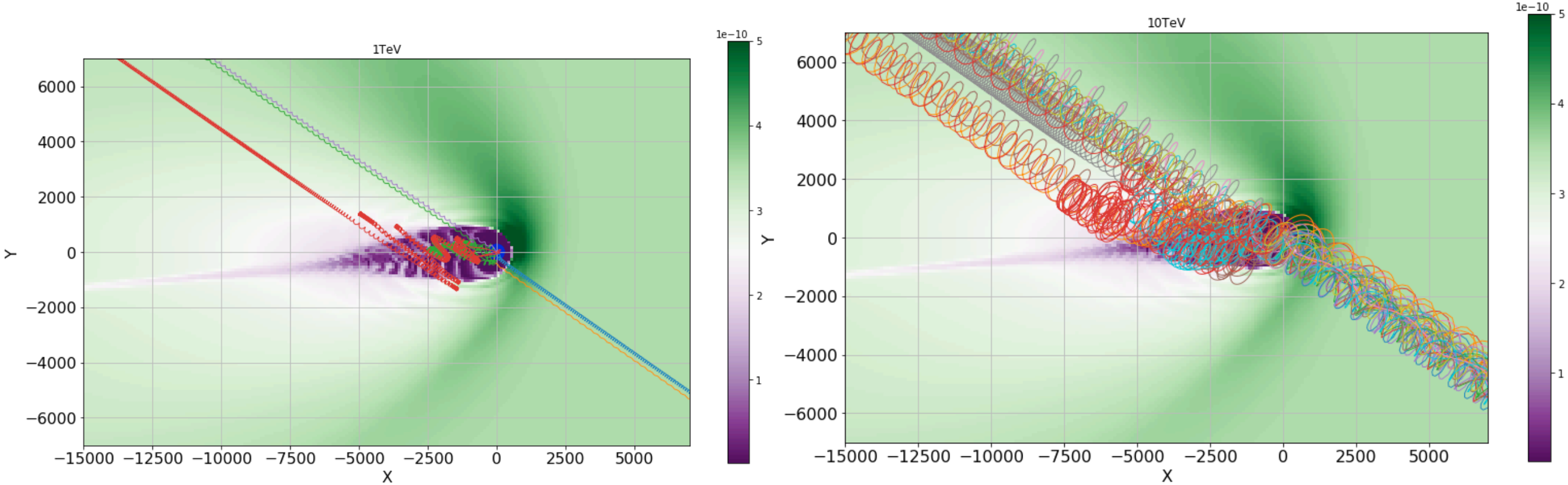

Meridional projection of the heliospheric magnetic field model described in (N. V. Pogorelov et al., ApJ 772 (2013) 2). The original simulation box dimension is 320 × 280 ×280 grid points (20 AU per grid point).

Lensing effect from the Heliosphere

Díaz-Vélez & Desiati 2019 PoS(ICRC2019)1076

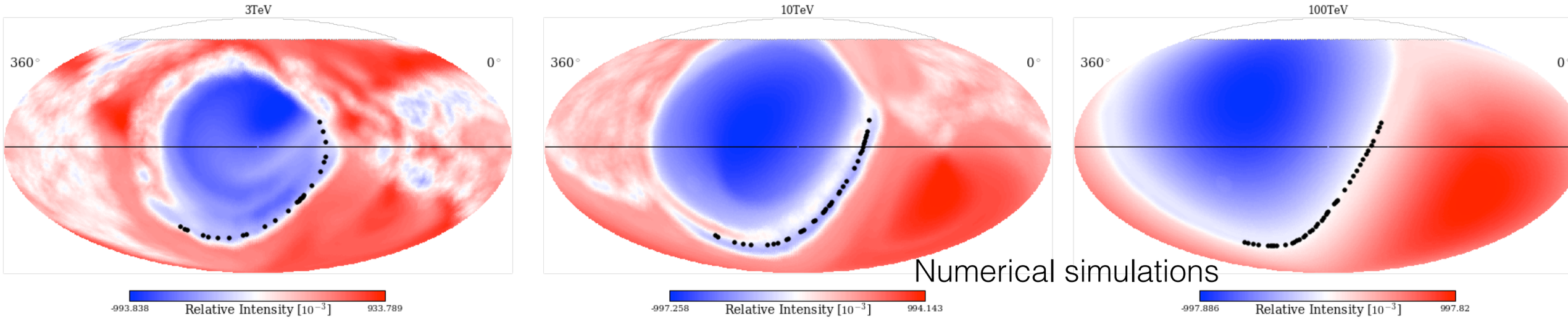

Numerical simulations

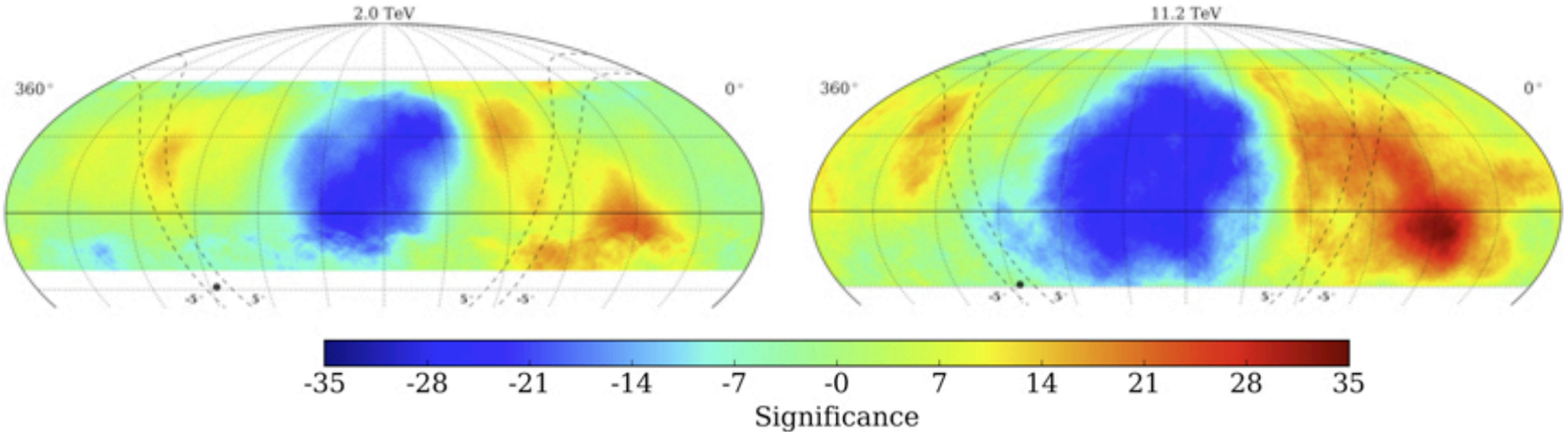

HAWC

A. U. Abeysekara *et al* 2018 *ApJ* **865** 57

Distribution of observed arrival directions of simulated protons at 1 TeV, 10 TeV, and 100 TeV resulting from an injected dipole oriented along the LIMF. The amount of distortion increases with decreasing energy.

The observed arrival distribution is the result of the combined energy distributions for all masses in data sample (but dominated by the peak of the distribution).

Energy Distribution

A. U. Abeysekara *et al* 2019 *ApJ* **871** 96

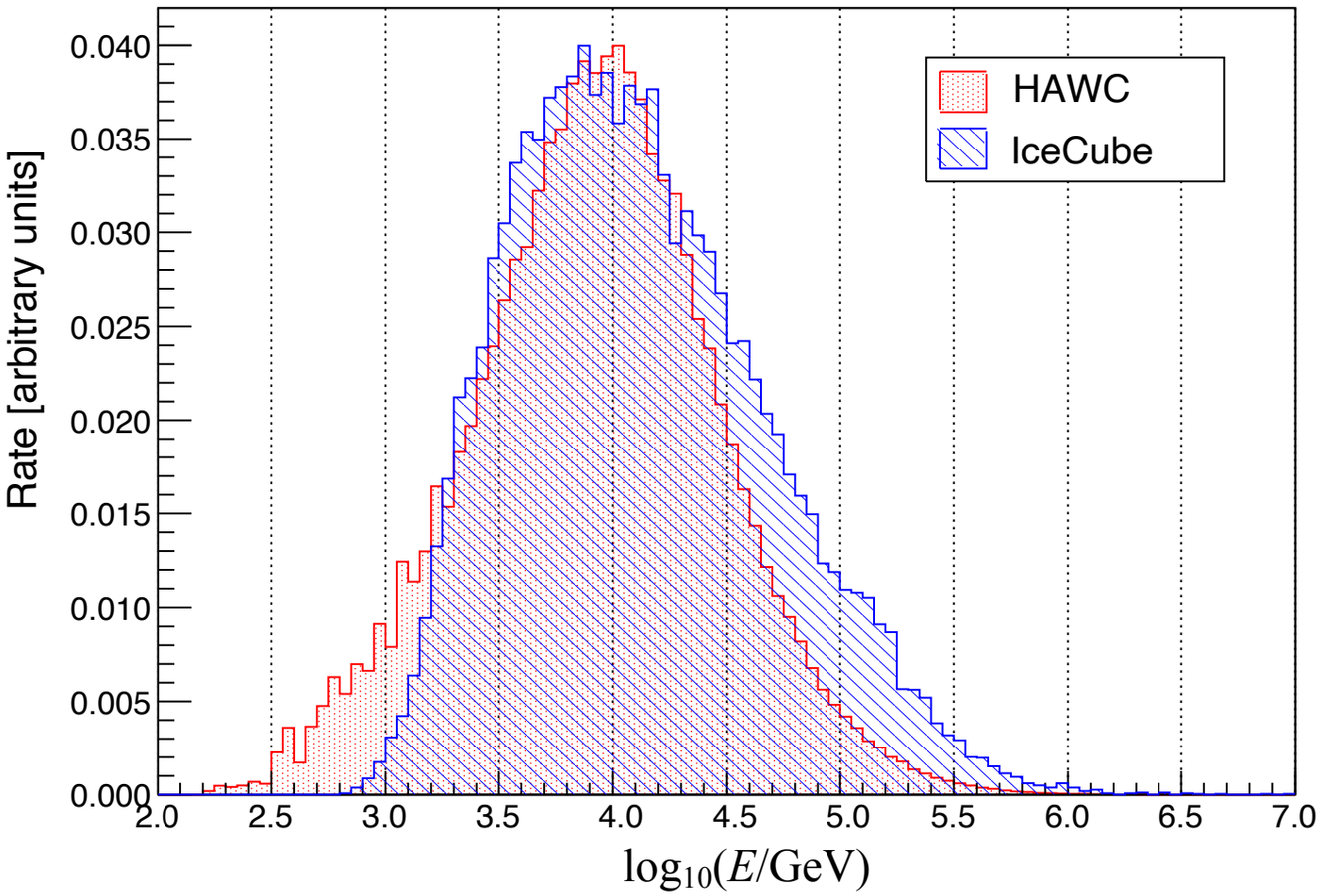

Composition

	IceCube	HAWC
Proton	0.756	0.616
He	0.195	0.311
CNO	0.028	0.047
NeMgSi	0.013	0.019
Fe	0.008	0.008

Median Energy

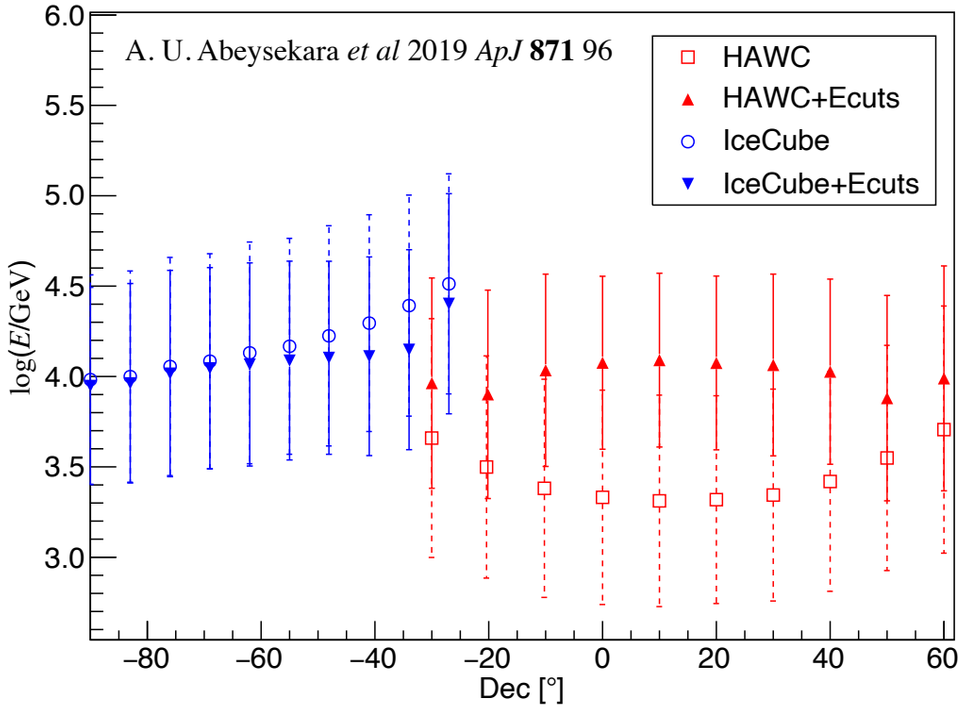

Energy distribution for datasets used in IceCube-HAWC analysis, based on Monte Carlo simulations. After cuts, both CR data sets have a median energy of approximately 10 TeV with little dependence on zenith angle. Before cuts, the median energy grows as a function of shower zenith angle and is largest in the narrow region of overlap between the two detectors.

Round-trip Test

Díaz-Vélez & Desiati 2019 PoS(ICRC2019)1076

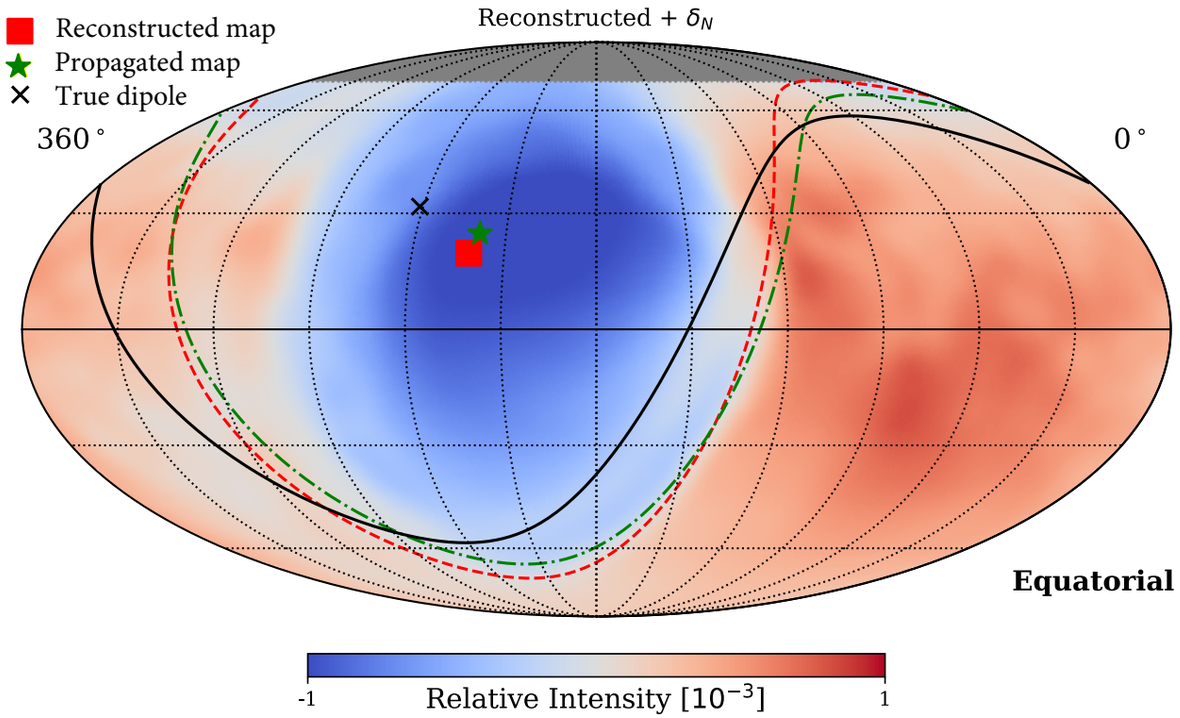

- Reconstructed map of the 10 TeV combined sample after propagation.
- The direction of the LIMF is indicated by the **X** and the corresponding magnetic equator is shown with a solid black curve.
- The inferred direction obtained by the same method used for the IceCube-HAWC analysis in A. U. Abeysekara *et al* 2019 *ApJ* **871** 96

The round-trip test reconstructs a dipole distribution from the mapping of local observed arrival distribution to the original injected dipole along the LIMF.

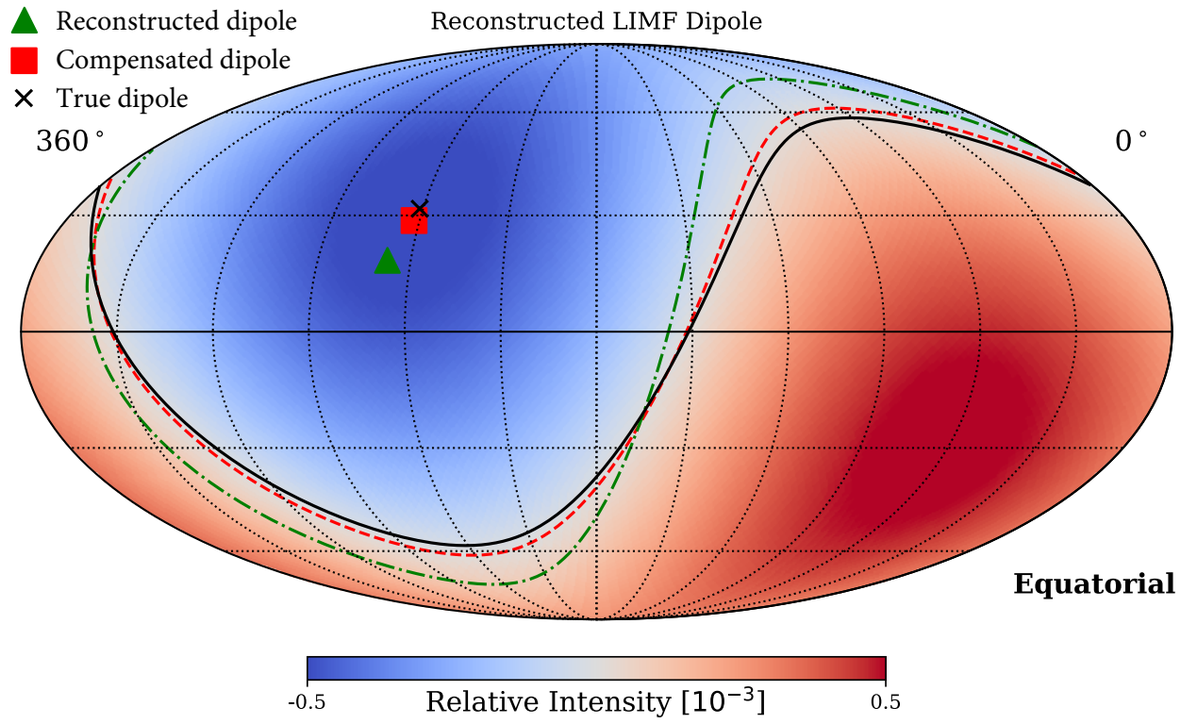

Inferred direction of the injected dipole is marked by the red square.

Measurement Biases on the Angular Power Spectrum

Díaz-Vélez & Desiati 2019 PoS(ICRC2019)1076

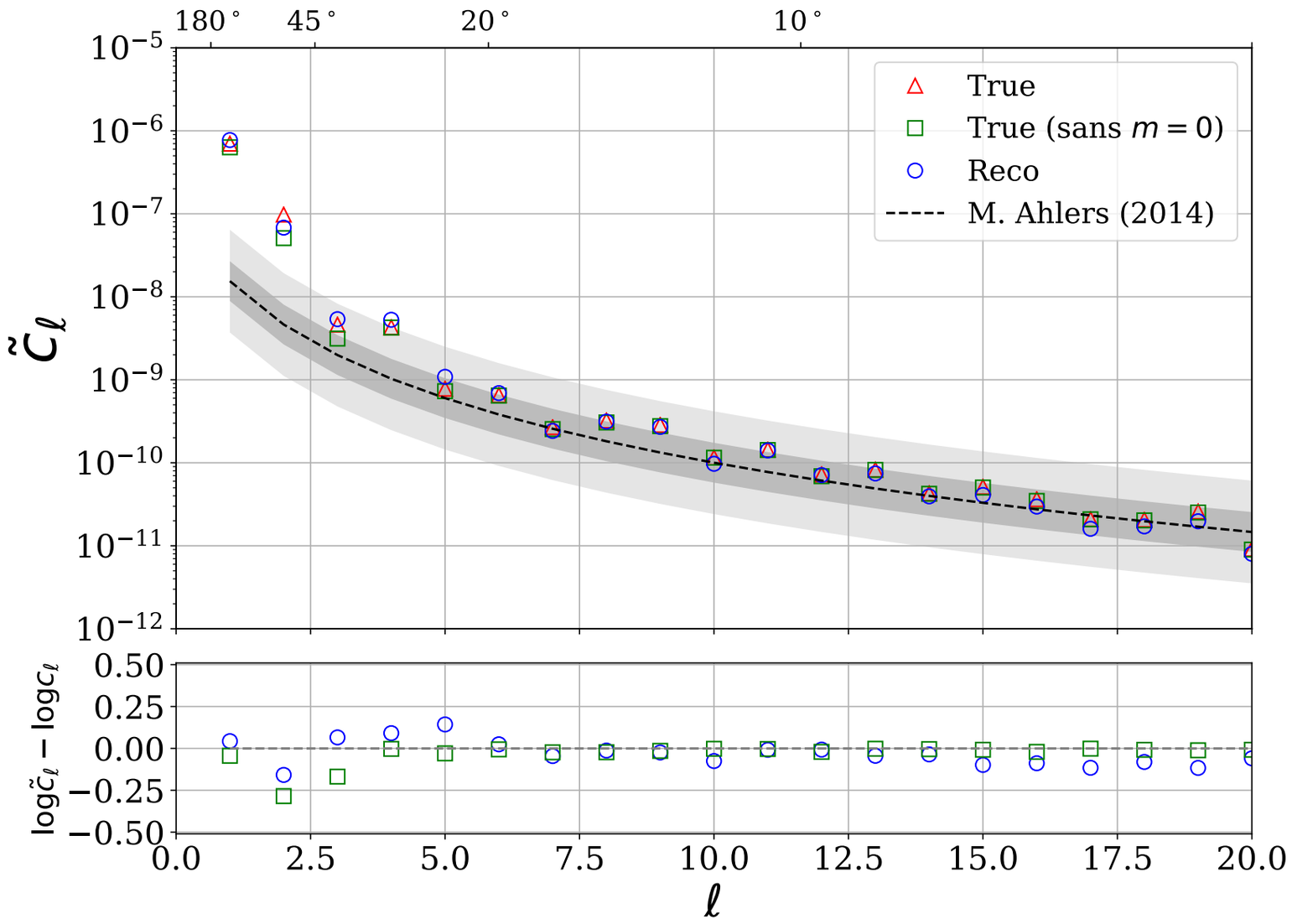

The angular power spectrum observed at Earth (simulation).
While most of the angular power is concentrated on the large scale anisotropy components, a hierarchical ordering of higher ℓ modes modeled in Ref. [29] is present and preserved in the reconstructed map.

Solar Dipole

Compton-Getting from Earth's motion around the Sun

$$\frac{\Delta I}{I} = (\gamma + 2)\frac{v}{c}\cos\theta$$

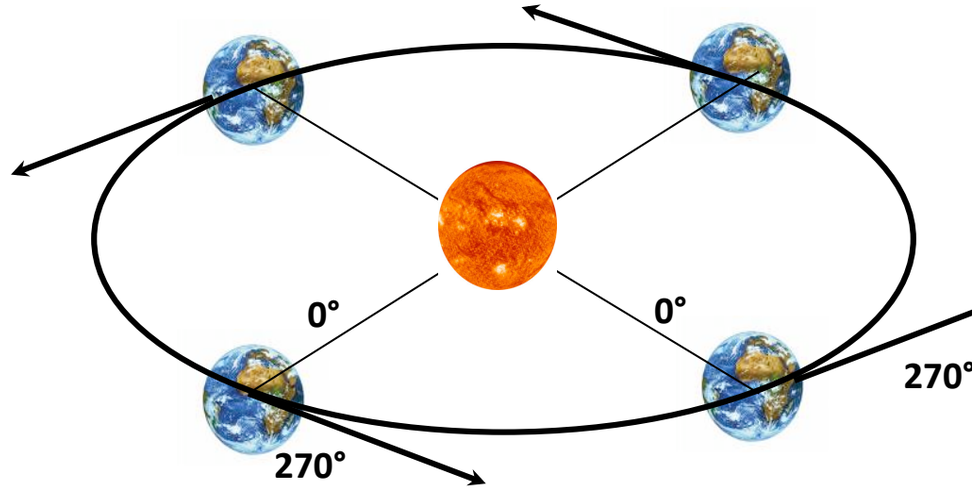

v = 29.8 ± 0.5 km/s

Compton & Getting, Phys. Rev. 47, 817 (1935)
Gleeson, & Axford, Ap&SS, 2, 43 (1968)

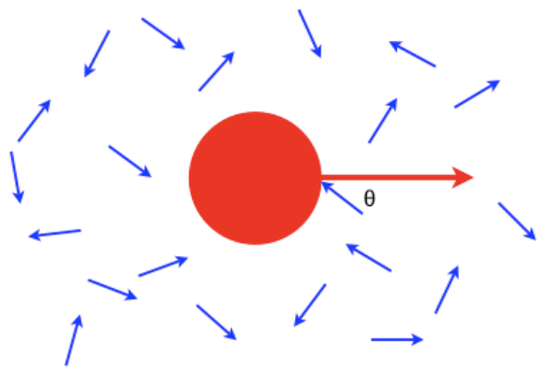

IceCube - Aartsen et al., ApJ 826, 220, 2016

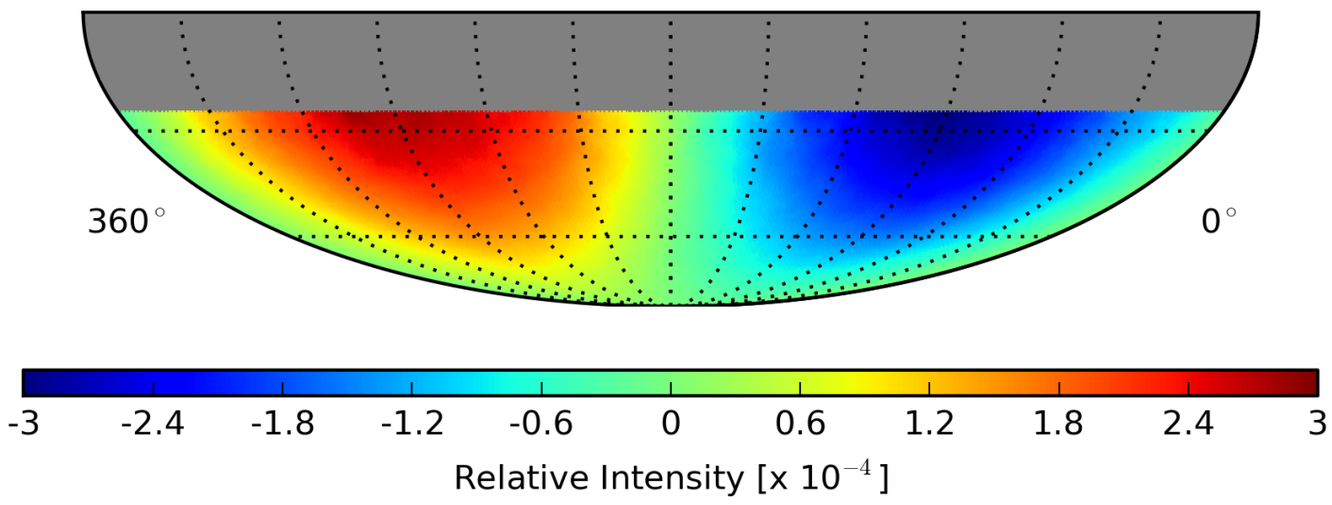

IceCube - Aartsen et al., ApJ 826, 220, 2016

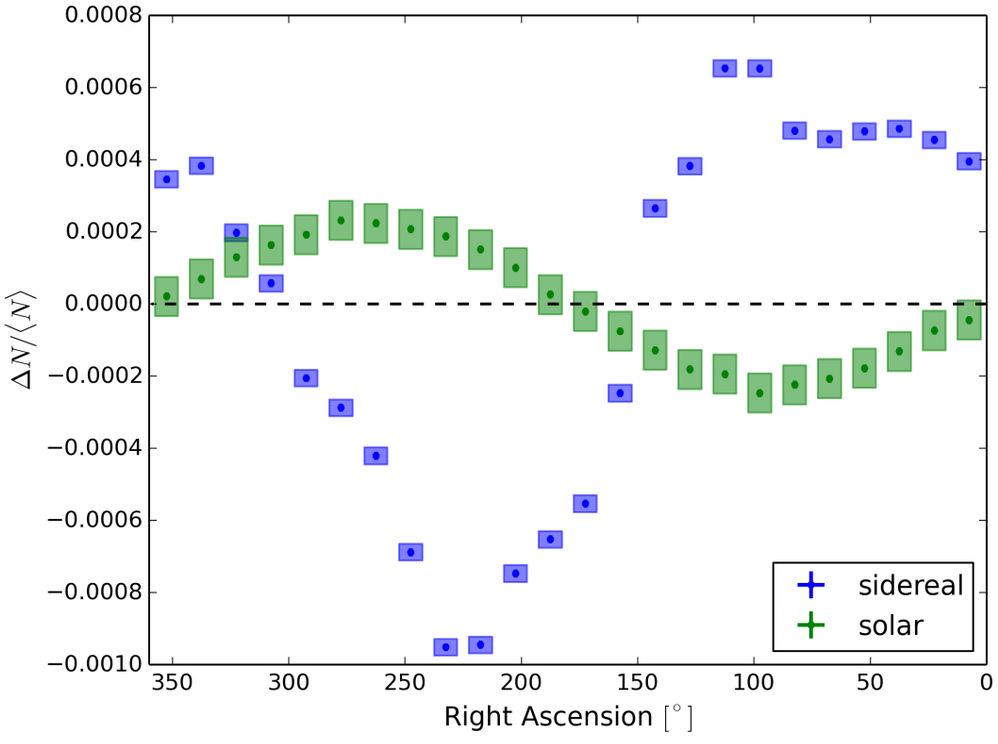

Interaction of the Solar and Sidereal frames

Díaz-Vélez, *et al* 2021 PoS(ICRC2021)085

Interference between solar and sidereal dipole anisotropies as observed in the sidereal reference frame at two different times during the year. The solar dipole introduces a bias in both amplitude and phase of the sidereal dipole

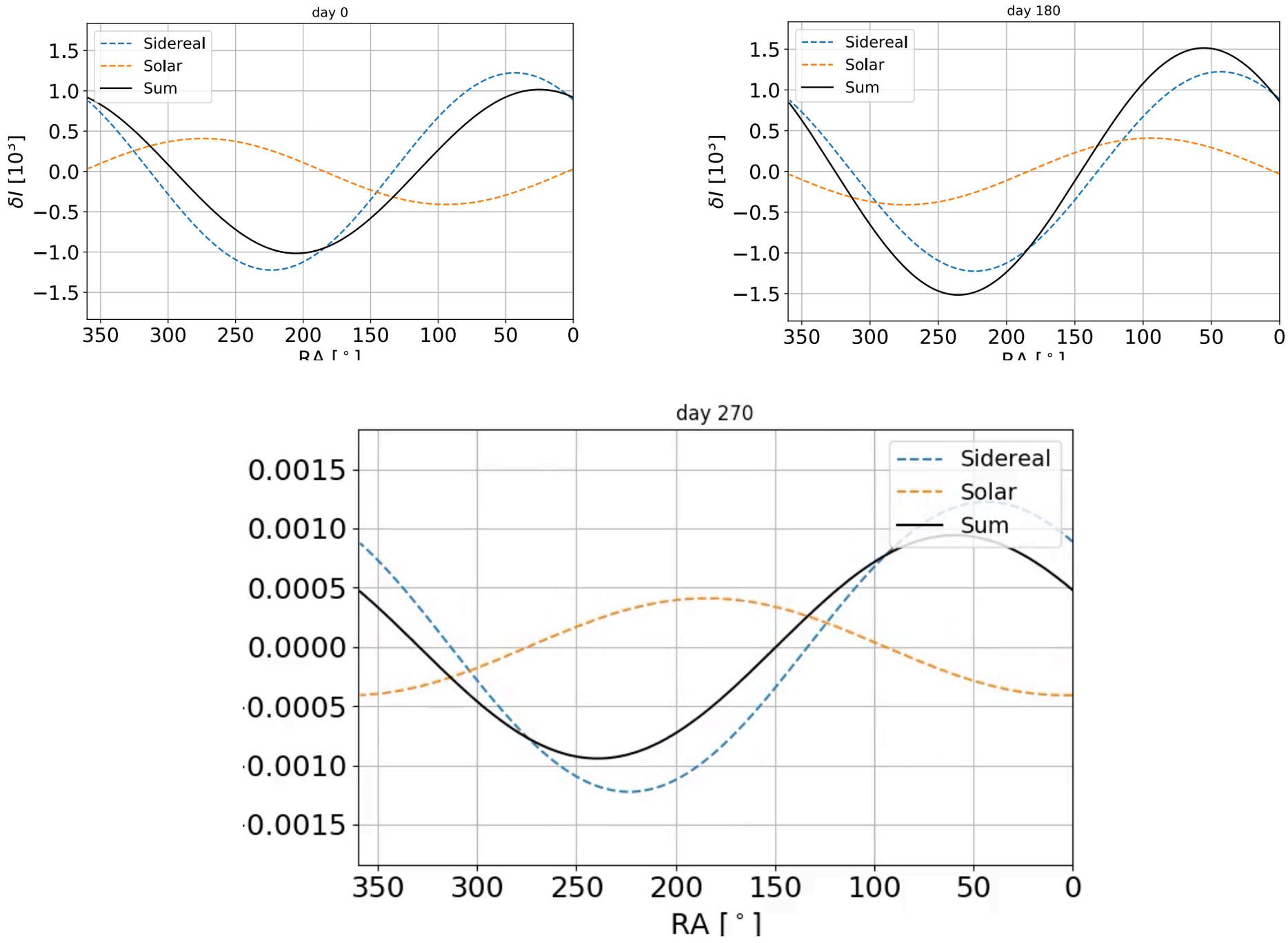

For a detector located at one of the poles with limited FoV, there is an attenuation of the solar dipole amplitude at either equinox because the velocity vector (anti-vector) is obscured below the horizon due to Earth's tilt.

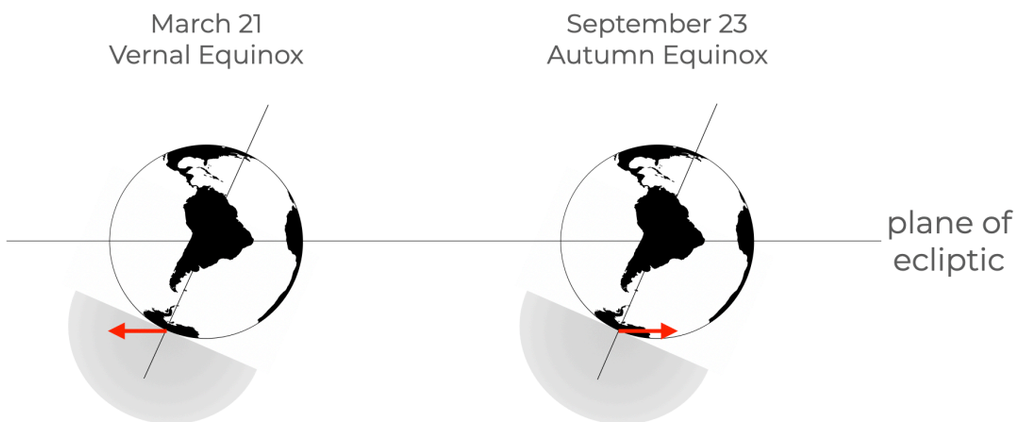

The rate of this change in amplitude is not symmetric because of the eccentricity of Earth's orbit.

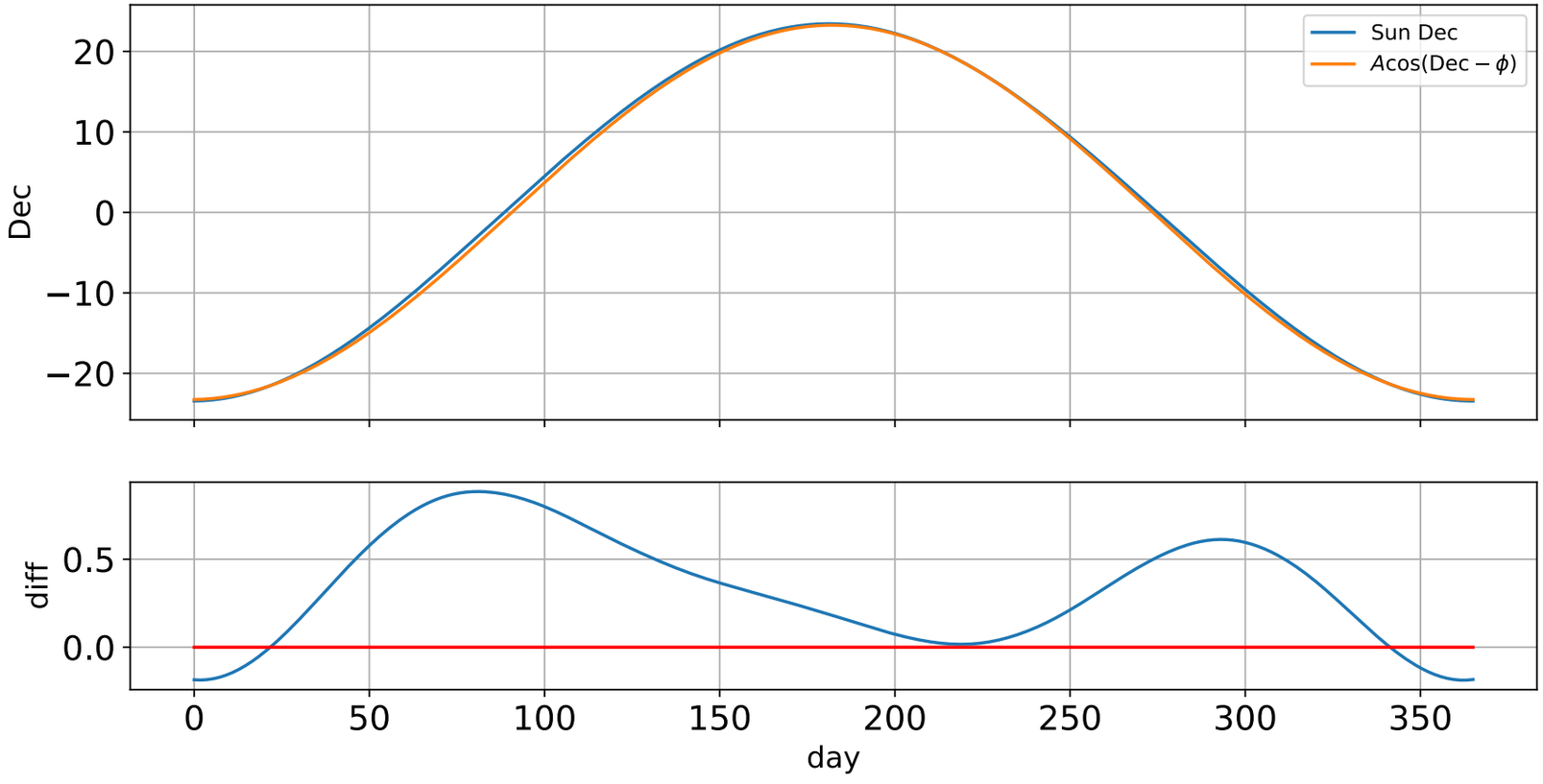

Díaz-Vélez, *et al* 2021 PoS(ICRC2021)085

Non-physical reference frames

Díaz-Vélez, *et al* 2021 PoS(ICRC2021)085

The mutual interference between modulations in the solar and sidereal frames produces frequency side-bands around the respective peaks in the frequency domain.

The side-bands overlap with the sidereal and solar frequencies, respectively, producing a deformation of the CRA.

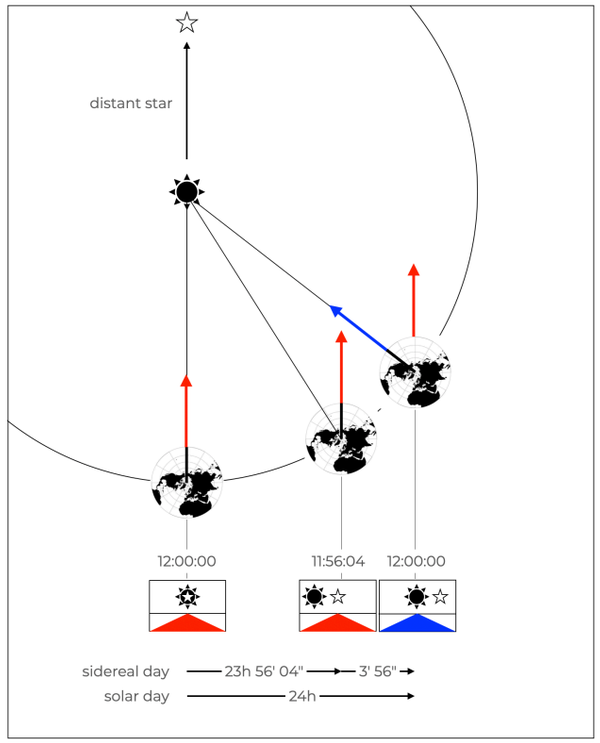

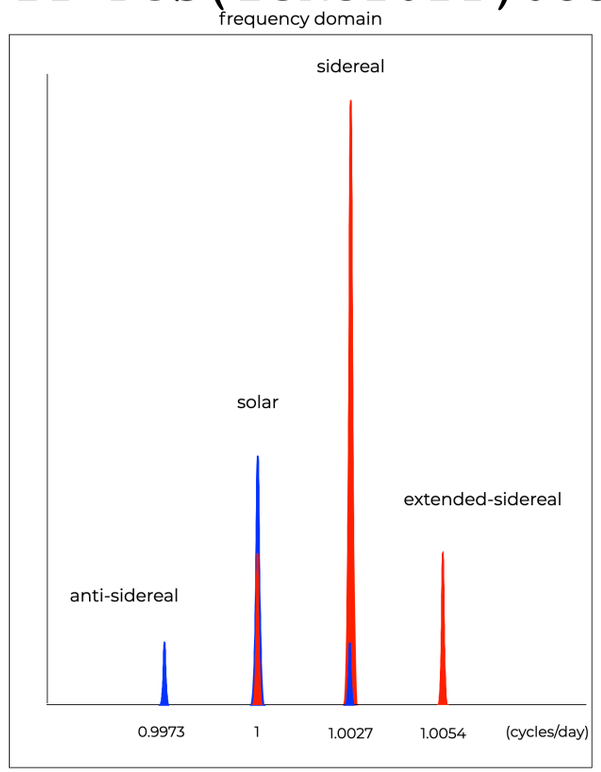

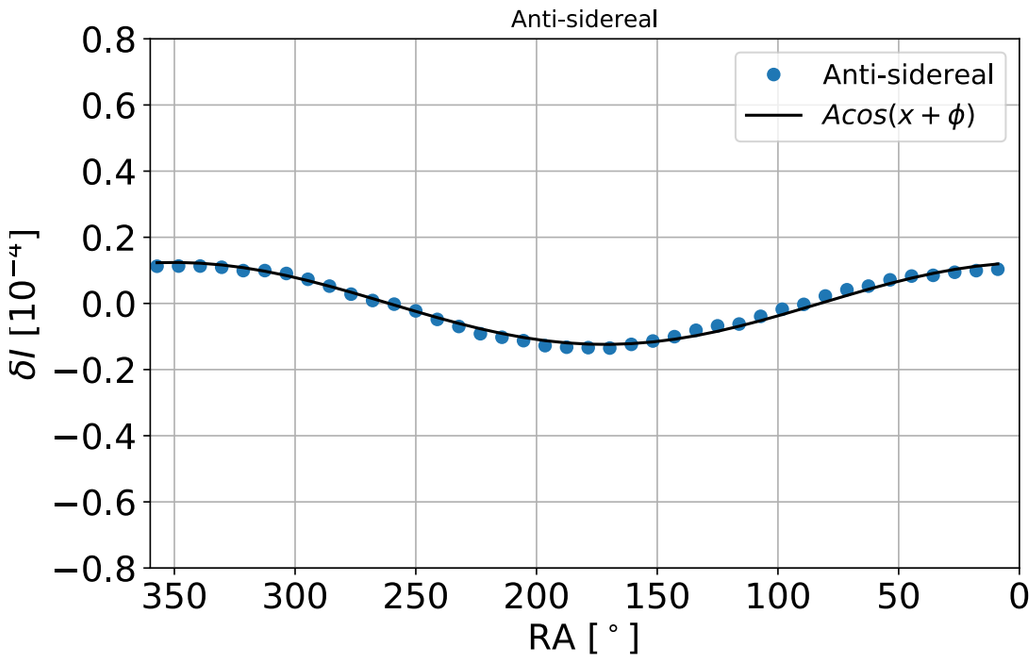

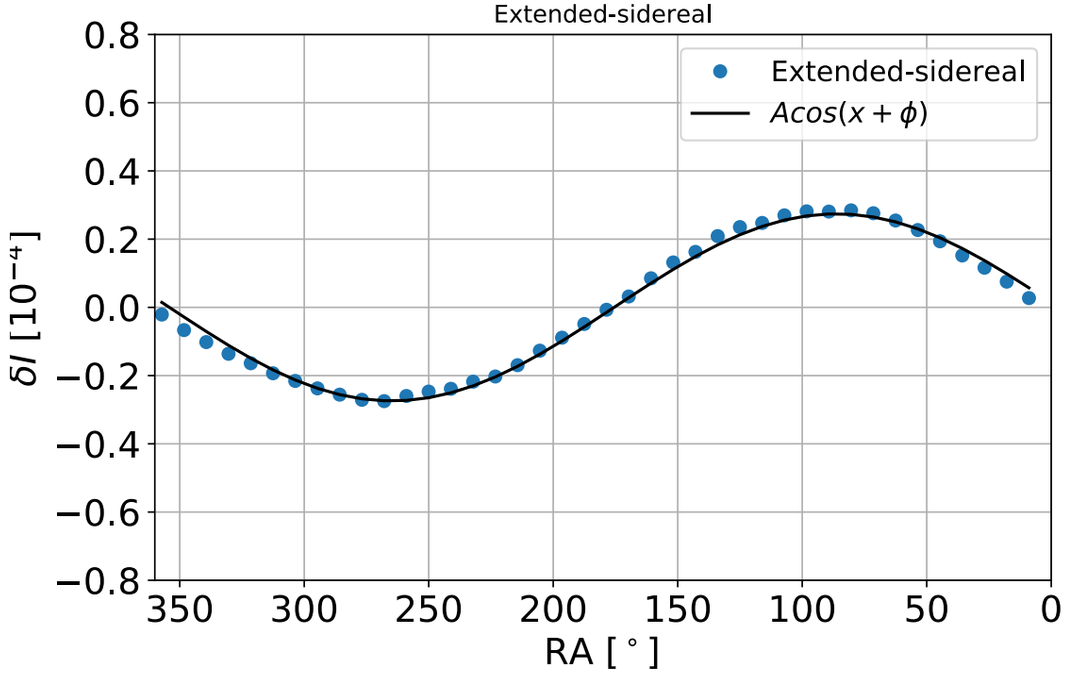

A toy simulation shows that, even with full coverage over 365 days, the solar and sidereal dipoles don't cancel out in their respective frames, resulting in a residual anti-sidereal (left), and extended-sidereal (right) distributions

An additional asymmetry in the amplitude of the solar dipole results the time dependence of the orbital velocity, primarily due to the eccentricity of Earth's orbit and to a lesser extent, from the orbit around the Earth-Moon center of mass.

The rate of this change in amplitude is also not symmetric because of the eccentricity of Earth's orbit.

Díaz-Vélez, *et al* 2021 PoS(ICRC2021)085

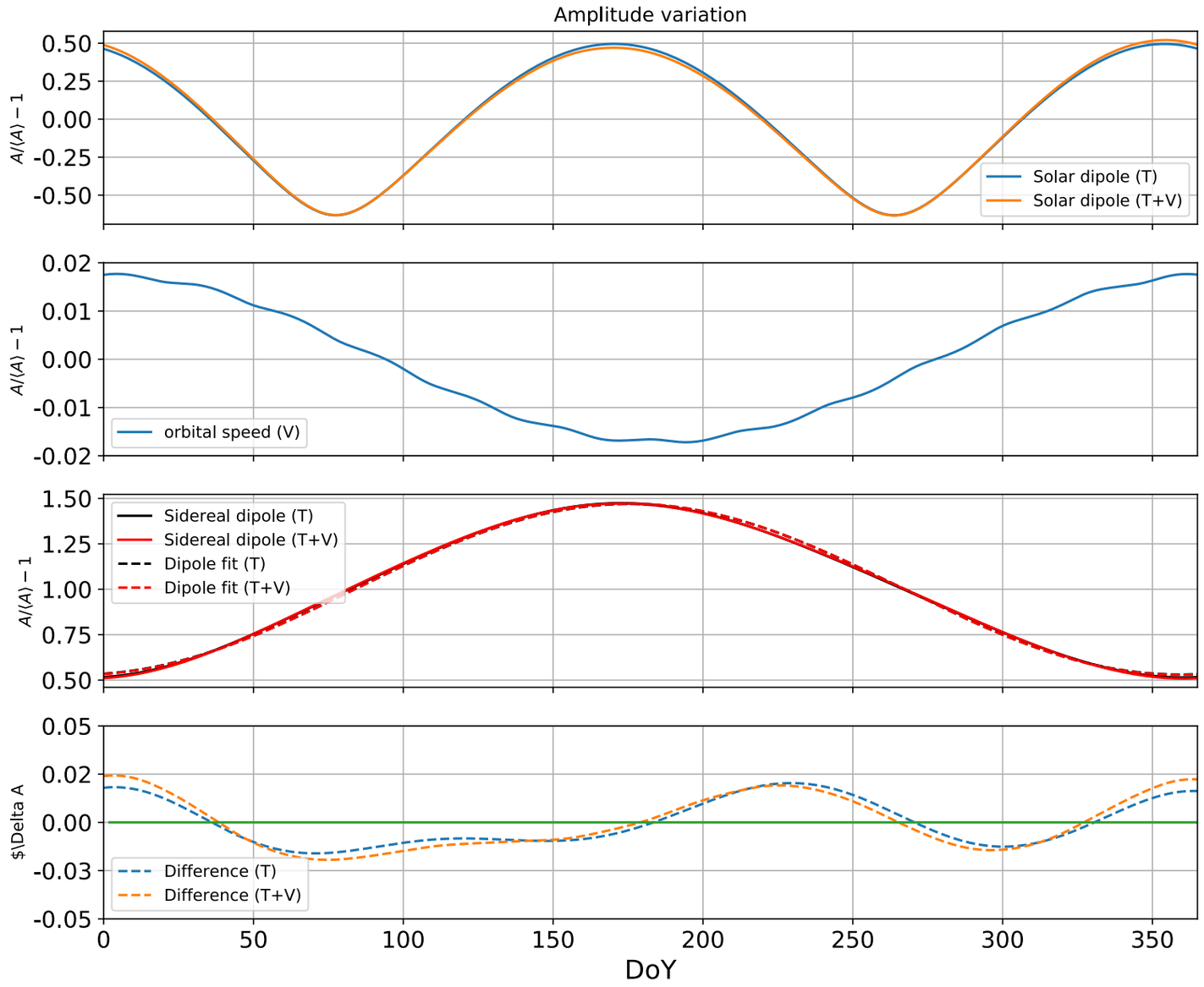

A dipole fit to the amplitude modulation over one year results in a residual signal due to the asymmetric nature of Earth's orbit.

Correcting for the Solar Dipole

The acceptance as a function of zenith angle along with a decreasing angular resolution for horizontal events results in a biased distribution for large zenith angles.

A simple correction based on the C-G equation would result in an over-correction for large zenith angles toward the horizon, and an under-correction towards 45º.

A compensation factor should include a correction based on the likelihood for an event to originate from a given direction.

By eliminating biases in the measurement of amplitude and phase of sidereal, and solar dipole distributions, this approach has the added benefit of eliminating the requirement for full integer year coverage and may provide a tool for probing yearly variations in the sidereal cosmic-ray arrival distribution.

Díaz-Vélez, *et al* 2021 PoS(ICRC2021)085

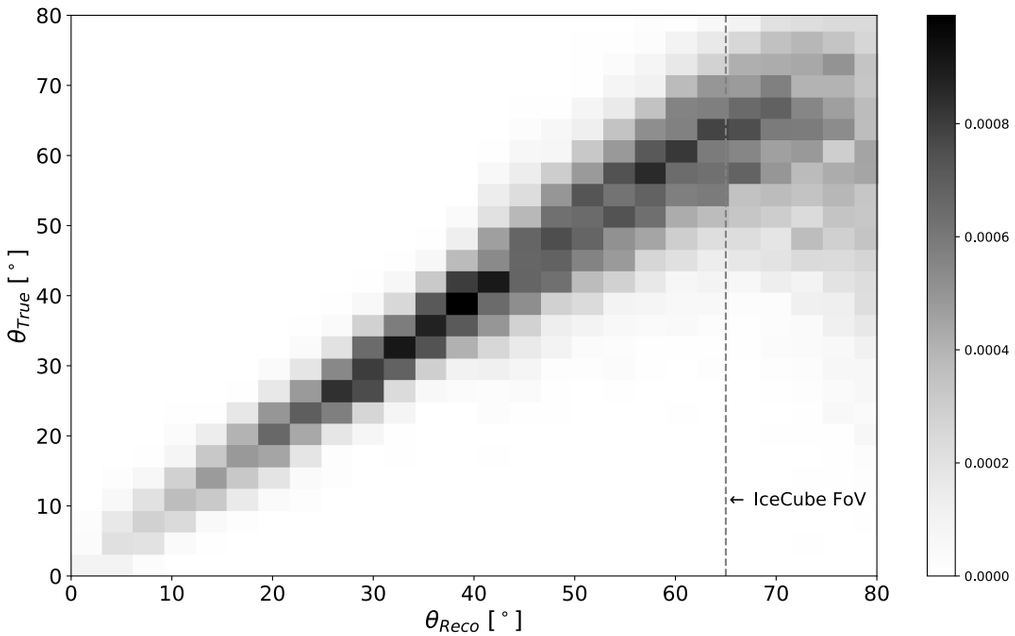

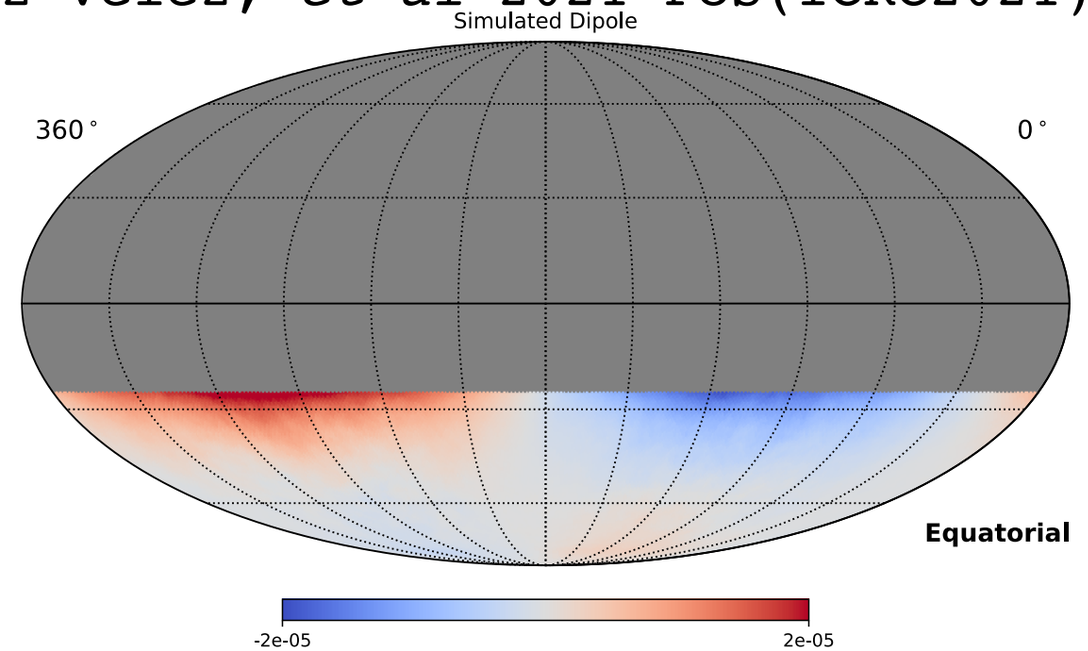

Left: Probability density function for a zenith angle θ to be reconstructed as zenith angle θ. There is an increasing bias towards the horizon at 90º that needs to factor into the solar dipole correction. Right: Zenith reconstruction bias results in an over-correction toward the horizon and an under-correction towards 45º

Summary

- Nearly full-sky cosmic ray arrival direction distribution from IceCube-HAWC study eliminates biases that arise from partial sky-coverage and provides better fit of phase and amplitude of horizontal component.

- Ground-based observatories are generally insensitive to cosmic-ray anisotropy variations that are symmetric in RA, i.e. only vary across declination bands (i. e. dipole only observed as a projection onto celestial equator).

- Geometric structures of 10 TeV anisotropy provides a tool to estimate the vertical dipole component.

- In round-trip simulations, the dipole amplitude, δ_P of the propagated map agrees to within 1% with the reconstructed dipole amplitude $\delta_R = \sqrt{\delta_H^2 + \delta_N^2}$ and in particular, we find that the estimate of δ_N agrees to within 2% of the true value for the specific heliospheric model in our study.

- The study suggest this approach is robust to energy and mass uncertainties from observations.